J. Fluid Mech. (1985), *vol.* 157, *pp.* 405–448
Printed in Great Britain

Developing turbulent boundary layers with system rotation

By J. H. WATMUFF†, H. T. WITT AND P. N. JOUBERT
University of Melbourne, Department of Mechanical Engineering,
Parkville, Victoria 3052, Australia

(Received 16 April 1984 and in revised form 3 December 1984)

Measurements are presented for low-Reynolds-number turbulent boundary layers developing in a zero pressure gradient on the sidewall of a duct. The effect of rotation on these layers is examined. The mean-velocity profiles affected by rotation are described in terms of a common universal sublayer and modified logarithmic and wake regions.

The turbulence quantities follow an inner and outer scaling independent of rotation. The effect appears to be similar to that, of increased or decreased layer development. Streamwise-energy spectra indicate that, for a given non-dimensional wall distance, it is the low-wavenumber spectral components alone that are affected by rotation.

Large spatially periodic spanwise variations of skin friction are observed in the destabilized layers. Mean-velocity vectors in the cross-stream plane clearly show an array of vortex-like structures which correlate strongly with the skin-friction pattern. Interesting properties of these mean-flow structures are shown and their effect on Reynolds stresses is revealed. Near the duct centreline, where we have measured detailed profiles, the variations are small and there is a reasonable momentum balance.

Large-scale secondary circulations are also observed but the strength of the pattern is weak and it appears to be confined to the top and bottom regions of the duct. The evidence suggests that it has minimally affected the flow near the duct centreline where detailed profiles were measured.

1. Introduction

The effect of streamline curvature in the plane of mean shear has long been known to cause surprisingly large changes in the structure of turbulent shear flow. Surface curvature has been the most common example and Bradshaw (1973) gives an excellent review of earlier work. Publications since that review include Hunt & Joubert (1979), Smits, Young & Bradshaw (1979) and Jeans & Johnston (1982). These studies have shown that even very mild curvature of the mean flow leads to substantial changes in the mean-velocity, turbulence-intensity and shear-stress distributions when compared with the corresponding straight flows. Many investigators, e.g. Tani (1962), have also reported the existence of longitudinal flow structures in the boundary layers over concave walls and have suggested that there could exist an array of counter-rotating turbulent vortices analogous to the Taylor–Görtler vortices in laminar boundary layers over concave walls. The effect of the Coriolis force is

† Present Address: Aeronautical Research Laboratories, Fishermen's Bend, Victoria, Australia.

equally striking but fewer investigations have been reported where the mean-streamline curvature is supplied by system rotation. These include Moore (1967) and Johnston, Halleen & Lezius (1972) who looked at the effect of rotation about a spanwise axis on fully developed turbulent duct flow, and Hill & Moon (1962), Moon (1964) and Koyama *et al.* (1979*a*, *b*) who studied the effect of rotation on boundary layers developing on the walls of a straight duct.

It is well known that there exists an analogy concerning the stability of laminar shear flow over curved and rotating boundaries and laminar flows with buoyancy. Various attempts have been made to extend the analogy to predict the observed effects of mean streamline curvature on the development of turbulent shear flows. In turbulent flow the similarity between the three types of body force is weaker since buoyancy forces depend on temperature fluctuations while the centrifugal and Coriolis forces depend on velocity fluctuations. Moreover the Coriolis force is proportional to velocity while the centrifugal force varies as the square of the velocity. Also the instantaneous Coriolis force is always normal to the instantaneous velocity vector and consequently is not associated with energy production (i.e. it is conservative) while the centrifugal force is non-conservative. Nevertheless, like the Reynolds analogy between heat and momentum transfer, the analogy has proved to be of practical use in prediction methods.

Various terms have been used to refer to the particular walls of a rotating duct. The names pressure and suction side originate from the pressure gradient due to the Coriolis force. The terms leading and trailing sides refer to the impeller blades in rotating machinery. The authors prefer to use the terminology destabilized and stabilized sides referring to the action of the Coriolis instability on the shear layers on these sides (see Bradshaw 1973). For the conditions as shown in figure 1 (*b*), the wall shown is the pressure, leading or, as we will refer to it, the destabilized side of the duct.

There is another, more indirect, way in which the action of system rotation can affect the layers on the sidewalls of a rotating duct. The shear layers that form on the top and bottom walls of the duct (i.e. perpendicular to the axis of rotation) are known as Ekman layers. The imbalance between the Coriolis force and the pressure force acting on the slower-moving particles in the top- and bottom-wall Ekman layers deflects fluid towards the stabilized side of the duct, causing secondary circulations to occur. Hill & Moon (1962) reported preliminary measurements of turbulent boundary layers developing on the walls of a rotating rectangular duct. The aspect ratio (height/width) of the duct was near unity and the results were significantly affected by secondary flows. A subsequent investigation was made by Moon (1964) where the aspect ratio of the duct was increased to 2:1 and the length increased so that measurements could be made at a number of streamwise stations. Marked increases in turbulence intensity, Reynolds stress and skin friction were observed on the destabilized side of the duct. Unfortunately these results were also affected by the large-scale secondary flows. The higher shear stresses observed in the destabilized layers could be due to the increased turbulent momentum exchange or to the removal of boundary-layer fluid by the secondary circulations. Similarly the lower shear stress on the stabilized side could be caused by secondary-flow depositions or by reduced momentum exchange. The inability to differentiate between these two effects is obviously undesirable. While the effects of secondary flows are important in many practical situations the most fundamental question about the effects of system rotation on turbulent shear layers is concerned with the Coriolis instability.

One method of studying the effect of the Coriolis instability in isolation is to

increase the aspect ratio of the duct so that the secondary circulations are moved further away from the duct centreline. Moore (1967) examined the relative importance of the Coriolis instability and large-scale secondary flows by conducting experiments in fully developed turbulent flow in rectangular ducts of different aspect ratios. The effects of rotation on the centreline mean-velocity profiles were significant in $\frac{1}{2}$:1 and 1:1 aspect-ratio ducts while much smaller effects were observed in 4:1 and $7\frac{1}{3}$:1 aspect-ratio ducts. Moore found that the mean velocity profiles obtained on the centreline of a 4:1 aspect-ratio duct are the same as those on the centreline of a $7\frac{1}{3}$:1 aspect-ratio duct within the experimental uncertainty.

Johnston, Halleen & Lezius (1972) also studied the effect of spanwise rotation on fully developed turbulent duct flow. The aspect ratio of the duct was 7:1 and the working fluid was water. Quantitative measurements were limited to mean-velocity profiles. The facility provided a unique opportunity to study the effect of rotation on the motions in the viscous wall region using wall-slot dye-injection and hydrogen-bubble-wire flow-visualization techniques. The non-dimensional wall-layer streak spacing was found to be the same as that observed by Kline *et al.* (1967) in a turbulent boundary layer. In the destabilized wall layer the rate of bursting was found to increase with increasing rotation rates, until, at moderate rotation rates, the bursting of the wall-layer streaks away from the wall appeared to evolve into spanwise arrays of roll cells which were seen to penetrate more than half way across the channel. The roll-cell structures were seen to form, wave about and decay in a very unsteady manner. Fresh dye released underneath the roll cells indicated that the formation of the wall-layer streaks appeared to be independent of the motions occurring above them. In the stabilized layers the rate of bursting was found to decrease for increasing rotation rates until at moderate rotation rates spot-like disturbances typical of laminar–turbulent transition were observed.

Koyama *et al.* (1979*a*) conducted an investigation into the effect of the Coriolis force on the turbulent boundary layers forming on the sidewalls of a constant-area straight duct with an aspect ratio of 7:1. Mean-velocity and streamwise-turbulence measurements were obtained with a normal hot wire at different streamwise stations, for a number of rotational speeds and for two free-stream velocities. Koyama *et al.* found that the boundary-layer development was promoted on the destabilized side of the duct and that the skin friction there was considerably higher than for zero rotation. Opposite trends were observed in the stabilized layers. Semi-logarithmic plots of the mean-velocity profiles in wall coordinates revealed that the viscous sublayer and buffer regions appeared little affected by system rotation. However, in the region where the logarithmic law of the wall is observed for zero rotation, the profiles appeared to lie on straight lines which deviate from the usual law. Koyama *et al.* used modified logarithmic-law-of-the-wall constants to describe their results and proposed that these were a function of an inverse Rossby number.

One of the advantages of studying fully developed duct flow is that the flow structure should be independent of the entry conditions and invariant with streamwise distance. For a given duct length, the width has to be narrow enough to obtain fully developed turbulent flow, which often conflicts with the need to have a duct that is wide enough to allow the flow to be investigated in some detail. Further, a wide duct tends to render negligible any flow disturbances caused by small variations in wall spacing or by the presence of probes. For a rotating duct the length is limited; Moore, for example, had to use a duct only 19 mm wide to get fully developed flow at his measuring station. This problem is avoided if the subject of study is the effect of rotation on developing turbulent boundary layers since the requirement here is

that the duct is wide enough to isolate the layers on either side by a non-turbulent core. However, the short length of a rotating duct requires the study of low-Reynolds-number developing turbulent boundary layers. It is surprising that there is a lack of reliable data for this flow, considering the frequency of its occurrence. While the scaling laws of the turbulent boundary layer can be regarded with some certainty at high Reynolds numbers the same cannot be said of the low-Reynolds-number case. It is apparent that a study should be conducted to ensure that a layer conforms to known properties before subjecting it to rotation.

The turbulent wall regions of fully developed duct flow and boundary layers are thought to be identical for zero rotation. However, the mean-velocity profiles of Koyama *et al.* in a rotating boundary layer show deviations from the logarithmic law of the wall that are of a different form to the results of Johnston *et al.* and Moore in rotating-duct flow. Part of the reason for the differences could be the higher resolution that is available in a turbulent boundary layer. Also, from the observations of Johnston *et al.* it is not completely certain whether the wall layers on the stabilized side of the duct are absolutely isolated from the roll cells emanating from the destabilized layers on the opposite wall. The study of the effect of rotation on an isolated turbulent boundary layer may provide some new insight into the influence of the Coriolis force.

2. Theoretical background

The momentum equations for an incompressible constant-property fluid observed in a rotating Cartesian coordinate system may be written as,

$$\frac{\partial \boldsymbol{U}}{\partial t}+\tfrac{1}{2}\boldsymbol{\nabla}(\boldsymbol{U}\cdot\boldsymbol{U})+(\boldsymbol{\omega}+2\boldsymbol{\Omega})\times\boldsymbol{U}+\boldsymbol{\Omega}\times(\boldsymbol{\Omega}\times\boldsymbol{r})=-\frac{1}{\rho}\boldsymbol{\nabla}P+\nu\boldsymbol{\nabla}^2\boldsymbol{U}, \tag{1}$$

where $\boldsymbol{r}$ is the radius vector, $\boldsymbol{U}$ and $\boldsymbol{\omega}$ ($=\boldsymbol{\nabla}\times\boldsymbol{U}$) are the velocity and vorticity vectors as measured in the rotating frame and $\boldsymbol{\Omega}$ is the rotation rate. The last term on the left-hand side can be expressed as the gradient of a scalar (the centrifugal pressure) and so be included with the absolute pressure gradient. The centrifugal pressure gradient is irrelevant to the dynamics of a constant-property fluid in the same way as the hydrostatic pressure gradient is irrelevant to water-channel flow for example. The effect of rotation is simply equivalent to adding uniform vorticity throughout the corresponding flow in an inertial frame. The extra term $2\boldsymbol{\Omega}\times\boldsymbol{U}$ is known as the Coriolis inertia force. If the equations are written using the more conventional convective derivative for the inertia forces and then non-dimensionalized by letting L, Ω^{-1} and U characterize typical length, time and velocity scales of a particular motion, then two important dimensionless parameters appear,

$$\frac{\partial \boldsymbol{U}}{\partial t}+Ro\,\boldsymbol{U}\cdot\boldsymbol{\nabla}\boldsymbol{U}+\frac{2\boldsymbol{\Omega}}{|\boldsymbol{\Omega}|}\times\boldsymbol{U}=-\boldsymbol{\nabla}P_r+E\boldsymbol{\nabla}^2\boldsymbol{U}. \tag{2}$$

The Ekman number $E=\nu/\Omega L^2$ is a measure of how the typical viscous force compares with the Coriolis force. It is essentially the inverse Reynolds number of the flow. The Rossby number $Ro=U/\Omega L$ is the ratio of the convective inertia forces to the typical Coriolis force and provides an overall estimate of the relative importance of the nonlinear terms. It is convenient to use the reciprocal values of these parameters to avoid the singularity when $\boldsymbol{\Omega}=0$.

Mager (1951) integrated the general case of the three-dimensional boundary-layer equations for layers developing on rotating boundaries. For two-dimensional layers

the momentum-integral equation is the same as that without rotation and offers little guidance to the mechanism by which rotation may affect the structure of a turbulent boundary layer. Prandtl (1931) made the first attempt to account for the effects of streamline curvature by multiplying the mixing length by a factor which is a function of a dimensionless curvature or buoyancy parameter. Prandtl's predictions were later found to be an order of magnitude less than subsequent experimental observations. More recently Bradshaw (1969, 1973) used the analogy between streamline curvature and buoyancy to argue that the factor affecting the apparent change in mixing length should depend on the gradient Richardson number. He then used the analogy to apply meteorological data to curved shear flows. He found that the use of a Monin–Oboukhov formula considerably improved the agreement between prediction and experiment for flow over curved surfaces provided the shear-layer thickness exceeds about 1/300 of the radius of curvature. So (1975) attempted to reduce the empiricism of Bradshaw's analysis by deriving an eddy-viscosity function from the turbulent-energy equation. He showed that the eddy-viscosity function can be put in the form of a correction factor for the mixing length and that for small Richardson numbers the Monin–Oboukhov formula is obtained. Bradshaw's analysis leads to a model for the mean flow which results in an extra linear term being added to the logarithmic law of the wall as follows,

$$U^+ = \frac{1}{\kappa}\ln y^+ + C - \frac{2\Omega\beta y}{u_\tau}, \tag{3}$$

where β is the Monin–Oboukhov coefficient $U^+ = U/u_\tau$ and $y^+ = yu_\tau/\nu$.

Some insight into the effect of rotation can be gained by considering the turbulent-energy equation and the turbulent-shear-stress transport equations (see Hunt & Joubert 1979). In contrast to the momentum equations, these equations contain extra terms representing identifiable additional processes owing to system rotation. The streamwise component of the turbulent-energy equation contains the extra 'production' term $2\Omega\overline{u'v'}$ while the component normal to the wall contains the extra term $-2\Omega\overline{u'v'}$. The transverse component (in the z-direction) is unaltered from the zero-rotation form. Summation of the components leads to the equation for the total energy, which is unaltered from the zero-rotation form. This is to be expected from the conservative nature of the Coriolis force. The extra terms may be interpreted as representing a conservative reorientation of the flow structure since energy is transferred without loss between the streamwise direction and the direction normal to the wall. The turbulent-shear-stress transport equation contains the extra 'production' term $2\Omega(\overline{u'^2}-\overline{v'^2})$. The change in the Reynolds stress relative to the case of zero rotation might be expected to be of the order $1+2\Omega\,\partial U/\partial y$ (see Bradshaw 1973). However, the observed changes in the Reynolds stress are found to be an order of magnitude greater than expected. In a developing flow, it is difficult to apply these equations since both the extra terms owing to rotation and the usual terms for a stationary flow would be changing with streamwise development. Our results suggest that the rate of boundary-layer development is affected by rotation.

3. Apparatus, instrumentation and techniques

The open-return tunnel is shown schematically in figure 1 (*a*). Air flow is provided by a two-stage axial-flow fan which is fixed one floor level above the rotating assembly. The flow passes into the rotating ductwork through a honeycomb which is fixed to the duct the purpose of which is to ensure that the entry flow becomes

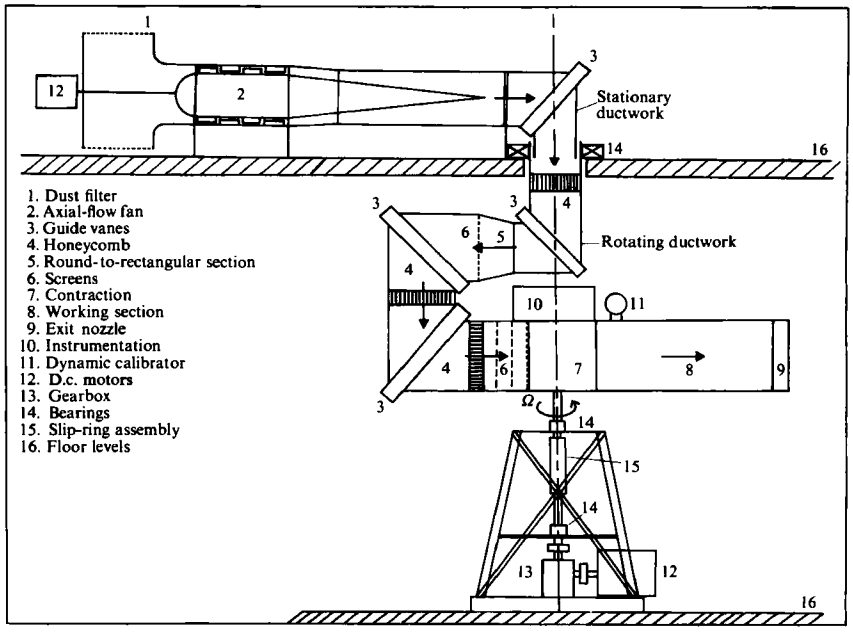

(a)

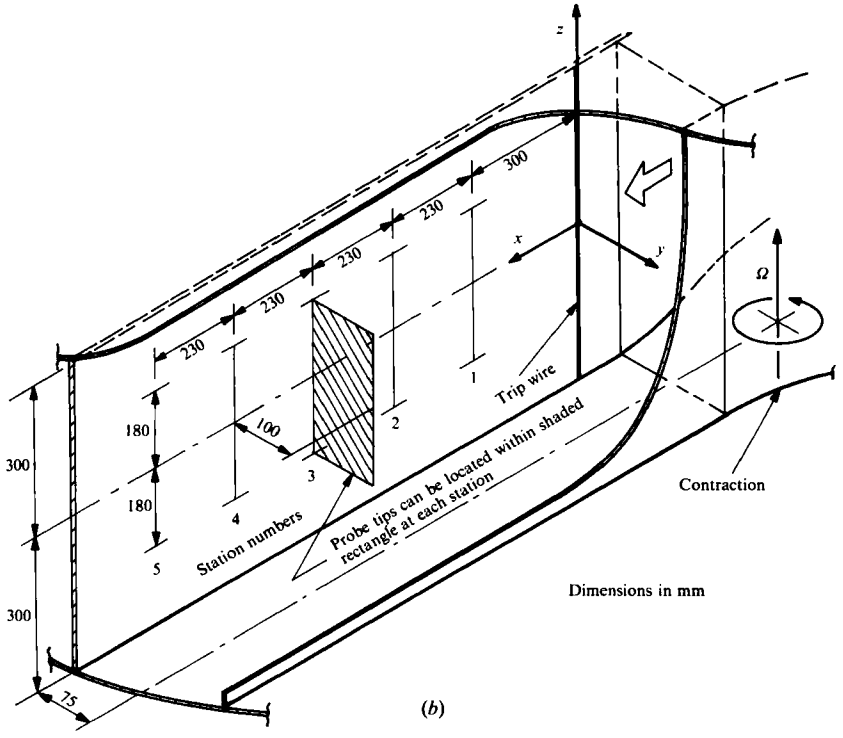

(b)

FIGURE 1. Schematic of apparatus: (a) overall view; (b) sectioned view of duct.

approximately irrotational relative to the ductwork under all conditions. The working section consists of a duct of rectangular section with two hinged straight Perspex sidewalls. The aspect ratio is 4:1. All measurements are taken in the boundary layers that form on one wall, the other having tightly fitting plugs to allow a bi-directional traverse to be installed at different streamwise stations. The tunnel can be rotated in either direction. The sidewalls of the duct have been adjusted so that the pressure-coefficient distribution on the duct wall and the free-stream-velocity distribution across the duct are uniform to within 1 % for all conditions reported in the experiments. Pressure coefficients have also been measured along the centreline of the contraction walls and there are no signs of flow separation. Negligible differences are observed between the values obtained when the tunnel is stationary and when it is rotating for the range of flow speeds used in the experiments. Figure 1(*b*) is a sketch of the duct showing the coordinate system and relevant dimensions. For all measurements presented here the rotational speed is 60 r.p.m.

The entry laminar boundary layers are tripped with a 1.5 mm diameter trip wire and reach a thickness of about 35 mm by the last station. Adopting the recommendations of Bradshaw (1965) for the final screen, the spanwise variation of the skin-friction coefficient in the layers was reduced to less than $\pm 2.5\%$ and the free-stream-turbulence intensity is less than 0.15 % for zero rotation. When it is rotating, the tunnel creates an external swirling flow in the laboratory which was found to cause unsteady puffing of the free-stream inside the working section. An end baffle is fitted to the exit of the duct when it rotates to minimize this effect so that the free-stream-turbulence intensity is then kept below 0.25 %.

Signals are extracted from the apparatus via a slip ring and brush assembly which also provides access for power and control signals. Noise contamination of the output signals by the slip rings and transmission lines is negligible. The traverse stepping-motor logic and drive circuits ride on the tunnel and are controlled by signals generated by a digital circuit that allows the probe to be moved to preselected positions. Pressures are measured with a differential electronic manometer mounted on the tunnel so that the irrelevant centrifugal pressure gradient is not detected. The output of the transducer is amplified prior to the slip rings as a precautionary means of further increasing the signal-to-noise ratio and mean values are obtained by electronically integrating the signals over a minimum period of 30 s. Mean-velocity profiles are obtained using a flattened total-head tube. The static pressure varies nonlinearly across the duct when it is rotating owing to the Coriolis inertia force. The iterative procedure given in the Appendix of Johnston *et al.* has been used to estimate the local static pressure. Wall distances are determined from the traverse display which is initially set after finding the point where the probe is just leaving the wall. Traverse backlash and deflections due to centrifugal forces are taken up under running conditions by lightly pressing the probe against the wall and then moving it away in 0.01 mm increments. The integrated output of the manometer is used to determine when the probe first leaves the wall. A constant wall-distance correction of 0.15 times probe height has been applied to all the boundary-layer data.

Accurate measurements of the shear velocity u_τ are of primary importance for the scaling of turbulent boundary layers. Techniques such as the Clauser-chart and Preston-tube methods should be applied with caution in flows subject to mean-streamline curvature. Deviations from the universal inner law occur in these flows, yet both techniques implicitly assume universal behaviour of the velocity profile to function correctly. The Clauser-chart method will indicate incorrect shear velocities if the mean flow departs from the logarithmic law of the wall. On the other hand the

Preston-tube method assumes a universal inner law from the wall outwards. Hence it is possible to select a tube diameter such that it is wholly immersed in the viscous wall region ($y^+ < 40$). Because the Coriolis forces are small and viscous forces dominate, it is reasonable to expect minimal departures from universal behaviour in this region. All shear velocities have been determined using a Preston tube the diameter of which ($d = 1.03$ mm) was selected such that the Reynolds number du_τ/ν ($= d^+$) lies between 20 and 40. Each experimental estimate of the shear velocity is determined from the ensemble average of three measurements before, and three after, each run. The Preston tube has been calibrated in a long ($L/D = 400$, $D = 0.1$ m) smooth-walled pipe from static-pressure-drop measurements over the full range of shear velocities to be experienced. The calibration agrees with that of Patel (1965) to within 0.5 % for higher values of d^+ but deviations as high as 3 % are reported for lower values.

Two constant-temperature hot-wire anemometers are mounted on the tunnel. A Disa 55P05 normal-wire boundary-layer probe is used to measure the streamwise turbulence intensity $\overline{u'^2}$ and a modified Disa 55P61 crossed-wire probe is used to measure the transverse turbulence intensities $\overline{v'^2}$, $\overline{w'^2}$ and the kinematic Reynolds shear stresses $\overline{u'v'}$, $\overline{u'w'}$. The tungsten filaments are replaced by Wollaston wire with etched sections 5 μm in diameter and 0.8–1.2 mm in length. A d.c. voltage is subtracted from each anemometer output and the resulting signal is amplified prior to the slip rings so that they lie between ±10 V over the range of velocities to be experienced by the wires. The frequency response of each anemometer is adjusted using square-wave injection to ensure a quadratic pole of optimum damping close to 20 kHz. After the slip rings the hot-wire system voltages are passed through fourth-order Krohn–Hite low-pass filters set at roll-off frequencies of 10 kHz.

For routine measurements, such as the determination of r.m.s. velocities analog data-acquisition techniques still retain considerable advantages over digital methods. Most small laboratory computers are incapable of repeatedly sampling a hot-wire voltage, converting the measurement to a velocity through some nonlinear calibration inversion process and then performing the necessary arithmetic to produce the final r.m.s. quantities in an acceptable period of time. Processing information with analog circuits results in faster data acquisition than digital methods. The authors constructed a hybrid system where unscaled mean and r.m.s. quantities are determined by analog techniques and then passed to a digital computer for scaling and further processing. The system has been thoroughly tested against a PDP 11-10 mini-computer by applying the same turbulence signals to both systems. The results were always within a few percent of each other. The hybrid system not only proved to be an order of magnitude faster but also gave more repeatable results.

For the normal wire, the amplified output is calibrated dynamically by shaking the probe sinusoidally in the free stream at ten representative velocities by a shaker attached to the tunnel. For the crossed-wire probe the amplified anemometer outputs are combined in such a way to produce a voltage sensitive only to streamwise velocities and a voltage sensitive only to transverse velocities. The small perturbation sensitivities to streamwise- and transverse-velocity fluctuations and to Reynolds-stress fluctuations are then determined directly and simultaneously by shaking the probe at 45° to the free stream. The final third-order polynomial calibrations are derived from the sensitivities. The method closely follows that described by Perry (1982). To eliminate one source of error in regions of high turbulence intensity the authors constructed an analog linearizer in the form of two third-order polynomial function generators using analog multipliers and squarers. The linearizer is set

according to the coefficients of the third-order polynomials after the dynamic calibration. In practice, we always dynamically calibrate the entire system (including the linearizer) before taking measurements. This reduces the possibility of the accumulation of small errors and provides an overall check on system linearity.

For each run, hot-wire-system drift is checked by integrating the output of the linearizer at a point in the free stream before and after taking measurements. Run data are rejected if the two inferred mean velocities differ by more than 0.5%. The initial distance of the wires from the wall is determined by using a flat plate attached to the probe holder to complete an electric circuit by touching the tip of a needle. Traverse backlash and any deflections due to centrifugal forces are taken up by lightly pressing the plate against the tip and then moving it away in 0.01 mm increments until the plate just leaves the needle. The initial wall distance of the normal wire is determined before each run by focusing a microscope with a graticuled eyepiece on the active section of the wire and its image in the perspex wall. For the crossed wires the wall distance is determined by focussing the microscope on the point where the wires appear to cross when viewed from the side. The microscope is also used to ensure that the three orientation angles of the crossed-wire probe relative to the free stream are very closely the same in both the traverse and shaker stings. The system voltages are used as a final check on the alignment which has always been found to be the same within a quarter of a degree of arc. The electric-contact method also serves to indicate the probe vibration during tunnel rotation is negligible.

The power spectral densities of signals from the normal hot wire are measured with a HP 3582A spectrum analyser which is interfaced via the HP-IB bus to a PDP 11/23 digital computer. The signals processed by the analyser are also simultaneously processed by our hybrid system so that ensemble averages of $\overline{u'^2}$ and U can be used in the non-dimensionalizing process.

4. Results and discussion

4.1. *Centreline results*

4.1.1. *Mean flow*

It was our intention to produce ordinary turbulent boundary layers that closely conform to known properties and then to subject these layers to spanwise rotation. Coles (1962) has pointed out that it is not as easy as is commonly supposed to produce such a typical turbulent boundary layer. The asymptotic state of full development, e.g. of the wake component, is approached in different ways depending on the transition process. This observation is of special significance to our work since the limited duct length confines our study to layers which have been promoted by a tripping device and whose wake parameters are still developing at the last streamwise measuring station. We decided to use a single trip wire and examine the properties of the developing boundary layers for three different free-stream velocities.

The properties of the zero-rotation layers will be examined in detail later but for now we will consider the deviations ΔU^+ of the rotating layer profiles from the logarithmic law of the wall in terms of (3). Throughout the work presented here the values of 0.41 and 5.0 have been assumed for the constants in the logarithmic law of the wall as recommended by Coles & Hirst (1968). The deviations are shown against non-dimensional wall distance in figures 2(*a*) and (*b*). To avoid cluttering the figures, only the results obtained at the last streamwise station are shown for the three free-stream velocities used throughout the experiments. In figure 2(*a*) least-squares

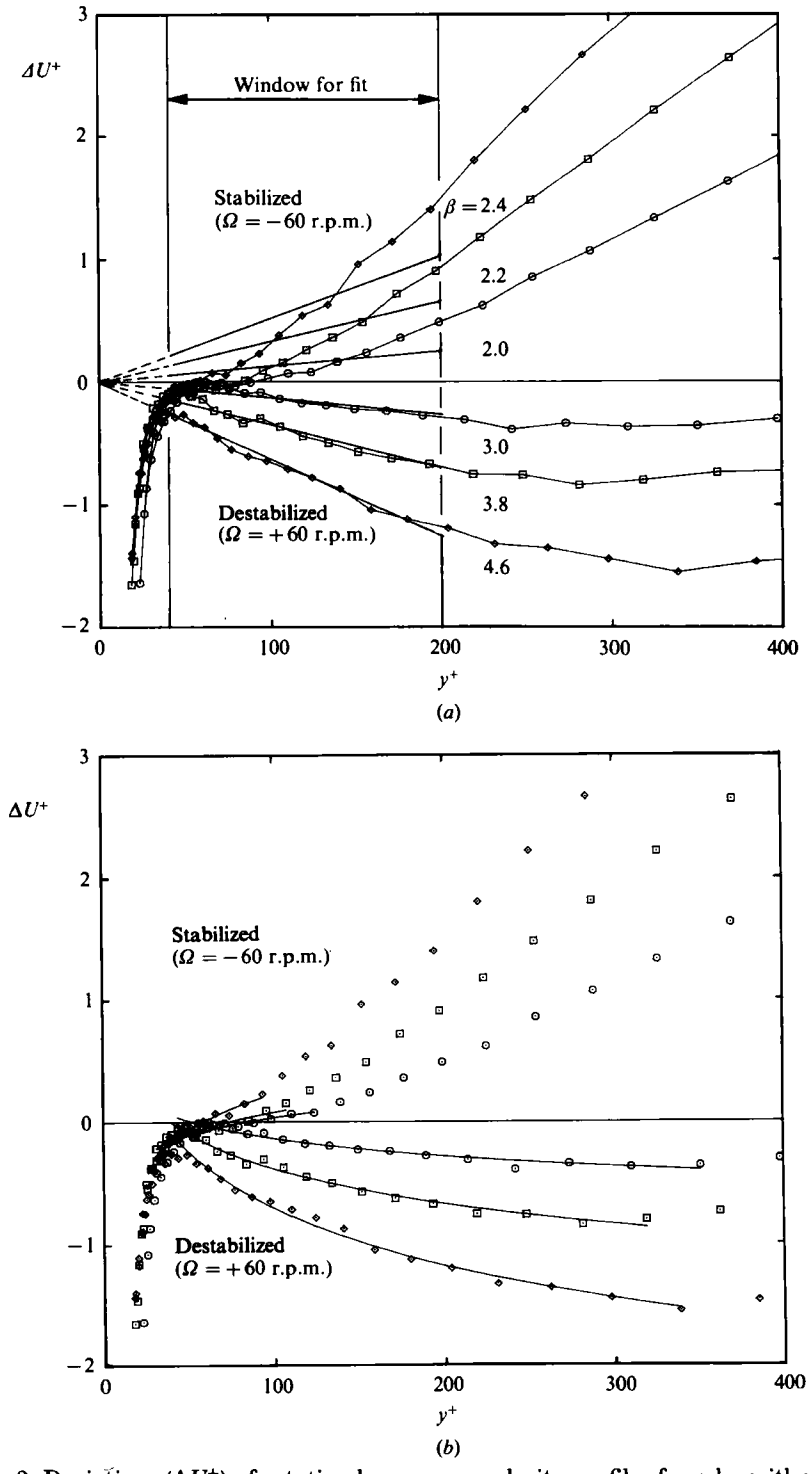

FIGURE 2. Deviations (ΔU^+) of rotating-layer mean-velocity profiles from logarithmic law of the wall. Last station only. (*a*) Lines of best fit through origin shown according to (3), i.e. linear variation of ΔU^+ with wall distance. (*b*) Lines of best fit according to (4), i.e. logarithmic variation of ΔU^+ with wall distance. Note better fit over larger range of y^+ in the destabilized layers. ◇, $U_1 = 7.5$ m/s; □, 10 m/s; ○, 15 m/s.

lines of best fit passing through the origin have been applied to the data in the range $40 < y^+ < 200$. The upper limit corresponds to that suggested by Bradshaw (1969) for (3) and the lower limit has been selected by the authors to correspond to the end of the viscous wall region. For the destabilized layers the lines fit the data reasonably well and correspond to values of β ranging from about 3 at the highest velocity to about 5 at the lowest velocity. The values are somewhat higher than those obtained by Bradshaw using the data of Johnston *et al.* For the stabilized layers the lines do not fit the data very well yet the squares of the correlation coefficients are around 0.96 and indicate linear behaviour. This is because the lines of best fit do not pass through the origin. The values of β range from 2 to 4 which are lower than those obtained by Bradshaw. So & Mellor (1972) found that $\beta = 4$ gives a better prediction of curved boundary-layer flows but So (1975) found that $\beta = 6$ gives a better overall prediction of all kinds of curved-flow data, meteorological data and rotating-channel data. Koyama *et al.* (1979*a*) report that β varies between 1 and 4 for their boundary layers. It seems that there is an inherent arbitrariness in the model since various workers have adjusted the value of β to get agreement with the limited amount of data available. It should be remembered that the model is based on the approximate similarity of the effects of buoyancy, centrifugal and Coriolis forces in turbulent flows and is limited by the inevitable defects of the mixing-length and eddy-viscosity hypotheses.

Rotation has a strong effect on the wall shear-stress distribution. Spanwise measurements of the skin-friction coefficient C_f' are presented in §4.2. For the destabilized layers there are large spatially periodic spanwise variations in C_f'. However, near the centreline these variations are smaller and are close to the mean value across the layer. The variation of C_f' along the centreline of the duct with Reynolds number based on momentum thickness R_θ is shown for the three free-stream velocities in figure 3. The zero-rotation results are close to the values recommended by Coles (1962) as being representative of a low-Reynolds-number turbulent boundary layer. The effect of rotation on these layers is also shown in the figure and, in all cases, the destabilized layers have larger values of C_f' and the stabilized layers have smaller values than the zero-rotation results. Each family of curves follows a pattern where the effect of rotation can be seen to increase with decreasing free-stream velocity.

One effect of mean flow three-dimensionality, generated by secondary flows for example, would be to cause a momentum imbalance in the streamwise direction. The mean-flow momentum equations have the same simple form for two-dimensional zero-pressure-gradient layers on a stationary and a rotating boundary. One way of checking for the effects of three-dimensionality of the mean flow is to compare C_f' obtained with the Preston tube to the streamwise derivative of the momentum thickness. Accurate estimates of the derivative are difficult to obtain since they require differentiation of a large number of profile estimates with the inevitable uncertainty due to experimental scatter. This is especially true in our situation since we have only five streamwise measuring stations. It was found that a second-order polynomial could approximate the variation of C_f' with streamwise distance with an accuracy of a few percent. The analytical integral of this expression has been used to predict the variation of the momentum thickness shown in figure 5. The unknown constant of integration, i.e. the effective origin of the layer, has been chosen such that the curves optimally pass through the data points. The agreement of the curves and the data points is excellent for the zero-rotation and stabilized layers; however, some small imbalances exist for the destabilized layers. These are largest for the results at 7.5 m/s. In §4.2 it is shown that longitudinal vortices in the mean flow coincide

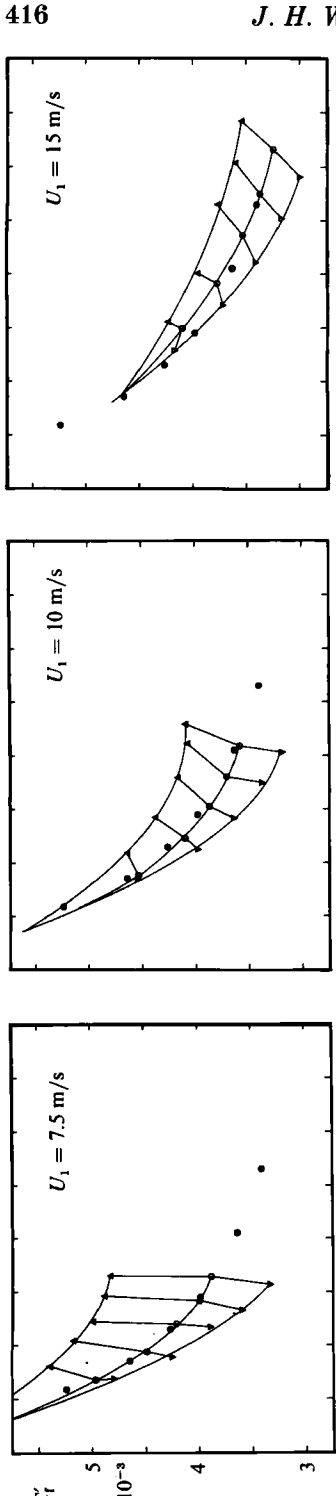

FIGURE 3. Development of C_f' with R_θ for three free-stream velocities and three rotation conditions used throughout experiments: △, destabilized (= +60 r.p.m.); ○, no rotation; ▽, stabilized (= −60 r.p.m.); ●, Coles (1962).

FIGURE 4. Development of strength-of-wake component relative to logarithmic regions shown in figure 6. (Symbols as in figure 3.)

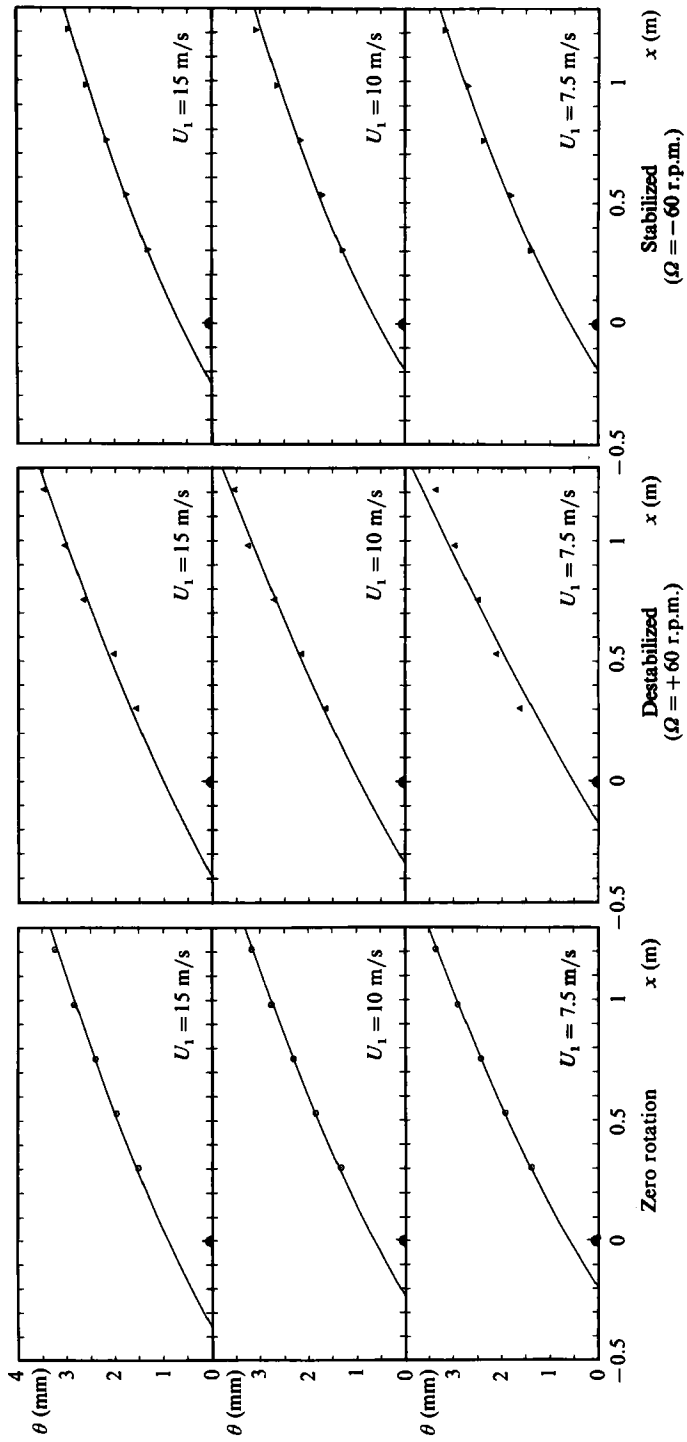

FIGURE 5. Momentum balance. θ *vs.* x for three free-stream velocities and three rotation conditions. Curves obtained from polynomial fit applied to experimental C_f' distribution agree with experimental data points. Symbol ▲ denotes streamwise position of trip wire.

with the spanwise variations of C_f' in the destabilized layers. Although the strength of the vortices is weak in this region it is not surprising to find a small deficit in the momentum balance. It is worth noting that the effective origin for the rotating layers is not markedly different from that of the zero-rotation layers, i.e. the downstream influence of the trip wire for the rotating layers is not significant.

It is appropriate to comment here on some of the final data-reduction techniques that we have developed and which have certain implications for our final results. Following Koyama *et al.* the authors wished to examine the mean-velocity profiles affected by rotation in terms of modified logarithmic law-of-the-wall constants. In order to give some credibility to the results a strategy that is free of subjective judgement was developed and firstly applied to the zero-rotation data. A least-squares logarithmic line is fitted to data points that lie within a selected window of $\ln y^+$. For each profile the upper and lower limits are chosen to maximize the window size under the restriction that the allowable deviation of the measured values of U^+ from the line should be within some specified tolerance. The authors were surprised to find that the tolerance on the deviations of U^+ could be made as low as 0.05, which is less than 0.5 % of the measured values of the mean velocities.

Watmuff, Witt & Joubert (1983) use a numerical Clauser-chart technique to make their zero-rotation profiles fit the logarithmic law of the wall with high precision. The technique optimizes u_τ and the wall distance of the closest data point to the wall, y_1. Relative distances between data points are unaltered. Pitot tubes are subject to wall-proximity effects and Watmuff *et al.* attempted to minimize experimental uncertainty by calibrating their Pitot tube in the zero-rotation layers. They then altered the two parameters so that the innermost portion of the profiles affected by rotation optimally fitted the zero-rotation profiles close to the wall. In all cases the values of u_τ required for this operation were within 1 % of the calibrated Preston-tube value and the alterations to y_1 were within 0.05 mm. The technique helped identify small errors in y_1 which were found upon subsequent reexamination of the recorded data. The mean-velocity profiles are now shown in figure 6, where the revised estimates of the initial wall distances and the calibrated Preston-tube values of u_τ have been used.

The least-squares strategy has been applied to all our profiles and the lines of best fit are shown as solid lines in figures 6 and 2 (*b*) corresponding to the ranges of y^+ that have been used. In all cases, the constants for the zero-rotation profiles are close to the accepted values of 0.41 and 5.0. A high degree of profile linearity in semi-logarithmic cordinates is indicated by the squares of the correlation coefficients which have values around 0.999. Since the correlation coefficients are of similar magnitude for the layers subject to system rotation and since the coefficients are larger than those obtained by assuming that the deviations vary linearly with wall distance (compare figures 2*a* and *b*), the authors feel justified, at least empirically, in using modified constants in the logarithmic law of the wall as the best way to describe the results, i.e.

$$U^+ = \frac{1}{\kappa_r} \ln y^+ + C_r. \tag{4}$$

One of the advantages of using the modified logarithmic-law approach is that the terminology used to describe ordinary boundary layers can also be given a precise definition when the layers are subject to system rotation. For instance, the strength of the wake component is a suitable parameter for characterizing the development of a low-Reynolds-number turbulent boundary layer. By defining a different logarithmic law, a corresponding definition of the strength of the wake component can

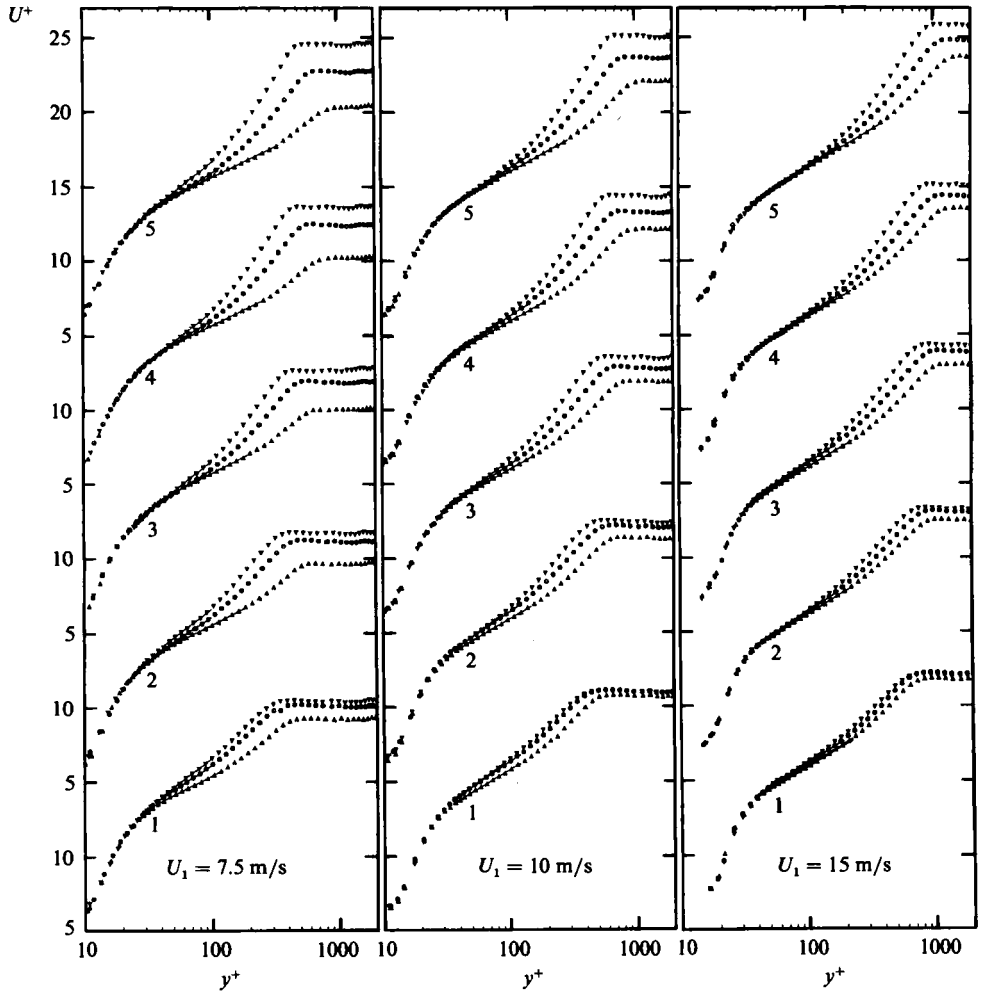

FIGURE 6. Development of mean-velocity profiles in wall coordinates for three free-stream velocities under the three rotation conditions. (Symbols as in figure 3.) Station numbers labelled. Lines show regions of logarithmic mean-velocity variation.

be made for layers subject to system rotation. The strength of the wake component relative to each logarithmic line of best fit is shown in figure 4 against R_θ. The results for the 7.5 and 10 m/s cases for zero rotation are typical of low-Reynolds-number boundary layers and follow the behaviour reported by Coles (1962). It is interesting to note that the 15 m/s case, presumably an overstimulated layer, has values that fall below his recommended values until after considerable development. Only the destabilized layers appear to be approaching asymptotic values that could be a characteristic of full development. For a given R_θ the stabilized layers have the largest strength of wake component while the destabilized layers have the smallest values.

Koyama *et al.* plotted their estimates of κ_r and C_r against the inverse Rossby number, $Ro_x = \Omega x/U_1$ (U_1 is the free-stream velocity and x is the distance downstream of the trip wire). Their results (kindly provided by H. Koyama) are shown in figure 7 (*b*) over the limited range of Ro_x encountered in our experiments. These values were obtained at one free-stream velocity and at two rotational speeds. In figure 7 (*a*) κ_r is shown against Ro_x for our data. Although there is quite a bit of scatter in the

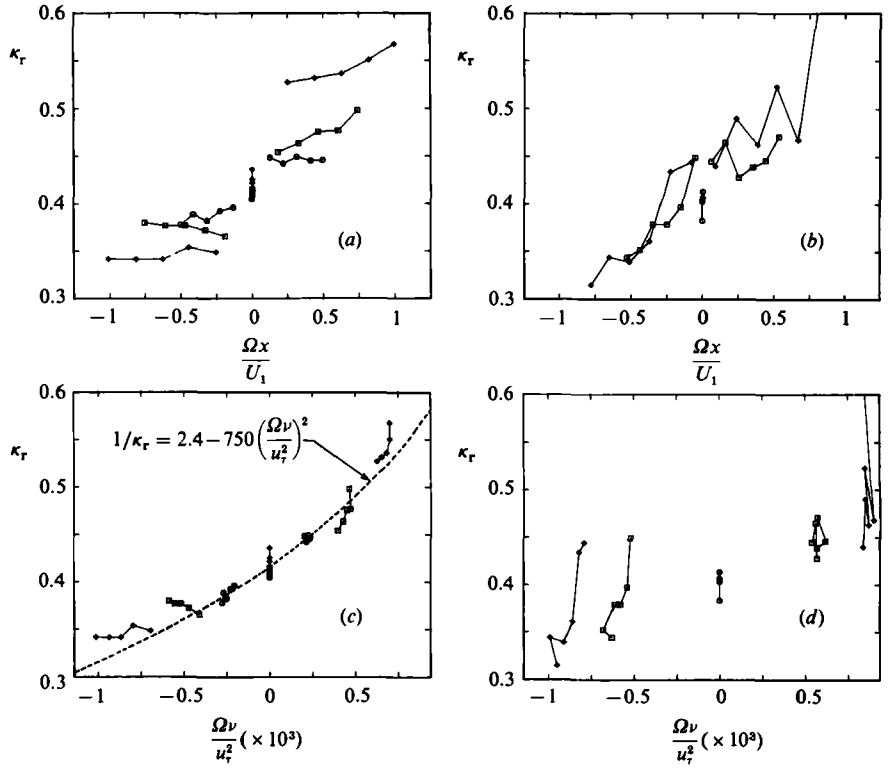

FIGURE 7. Variation of modified logarithmic-law constant κ_r with rotation parameters. (*a*) and (*c*), present investigation, $\Omega = \pm 60$ r.p.m.: ◇, $U_1 = 7.5$ m/s; □, $U_1 = 10$ m/s; ○, $U_1 = 15$ m/s. (*b*) and (*d*), Results of Koyama *et al.* (1979*a*), $U = 10$ m/s: ◇, $\Omega = \pm 150$ r.p.m.; □, $\Omega = \pm 100$ r.p.m.; ○ = no rotation.

results, there does appear to be a trend for different free-stream velocities. Since the region where logarithmic behaviour is observed is close to the wall it could be more appropriate to use the quantities ν/u_τ and u_τ for the length and velocity scales. Then the inverse Rossby and Ekman numbers both become $\Omega\nu/u_\tau^2$ which can also be interpreted as the ratio of the rotation rate to the mean sublayer vorticity. Figure 7(*c*) shows our results with this scaling. For small $\Omega\nu/u_\tau^2$, the empirical relationship

$$\frac{1}{\kappa_r} = 2.4 - 750\,\frac{\Omega\nu}{u_\tau^2}$$

fits our results reasonably well. Although the result for our data looks promising the results of Koyama *et al.* show increased scatter when plotted against this parameter (see figure 7*d*). Many combinations of different length and velocity scales were tried but the best results for our data is that shown in figure 7(*c*). Similar results are obtained for C_r which are not shown here. Since the layers of Koyama *et al.* were forming on the walls of a duct of constant cross-sectional area the boundary layers must have been subject to a mild favourable pressure gradient. Also the free-stream turbulence intensity of their duct was around 2%. The modified logarithmic-law constants could be functions of more than one variable; however, later measurements by Koyama *et al.* (1979*b*) indicate that there are spanwise mean-flow inhomogeneities near the centreline of their destabilized layers. In §4.2 profiles are presented which

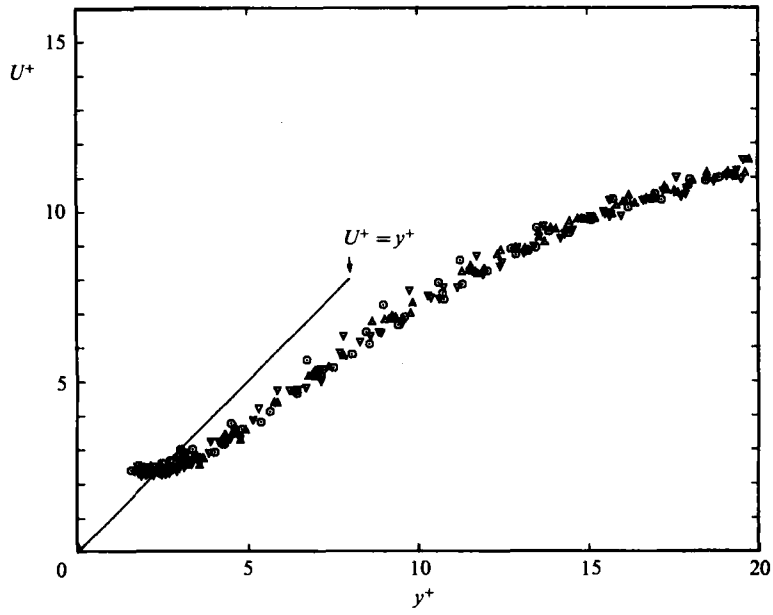

FIGURE 8. Mean-velocity profiles in wall region, U from normal hot wire, u_τ from Preston tube, 21 profiles. Deviations from sublayer profile are independent of streamwise location, free-stream velocity and rotation condition. (Symbols as in figure 3.)

have been obtained away from the centreline where there are spanwise variations in C_f' in the destabilized layers. Different behaviour is observed.

In order to provide a cross check on the Pitot-tube measurements mean-velocity profiles were also obtained with the normal hot wire. Considerable effort was made to obtain the most accurate measurements possible. In particular an attempt was made to get precise measurements in the viscous sublayer. Figure 8 shows the results of 21 profiles obtained under different rotation conditions, at different streamwise stations, for the three free-stream velocities used in the experiments. Although there is no discernible trend in the results for different rotation conditions, the data do not follow the sublayer relationship. The Preston-tube estimates of u_τ are about 12% higher than that indicated by the velocity gradient near the wall. Similar differences have been observed by Blackwelder & Haritonidis (1983) in a turbulent boundary layer who found that the estimate of the u_τ from the slope of the logarithmic region was about 15% higher than that determined by the velocity gradient near the wall. The authors could find no evidence to suggest that the anomaly is caused by errors in wall distance, calibration or wall-proximity heat-transfer effects for $y^+ > 5$. The non-dimensional length of hot-wire filaments is between 20 and 40 for these measurements. The hot-wire data estimates of the logarithmic-law constants are all slightly lower than those found with the Pitot tube (e.g. $\kappa \approx 0.39$ from hot-wire data, $\kappa \approx 0.41$ from Pitot-tube data in the zero-rotation layers), while a similar fit over the same range of y^+ is obtained for all profiles.

4.1.2. *Turbulence measurements*

The streamwise development of C_f' and the strength of wake components for the zero-rotation layers at the free-stream velocities of 7.5 and 10 m/s conform to documented properties of a low-Reynolds-number turbulent boundary layer. The layer with a free-stream velocity of 7.5 m/s shows the greatest effects caused by

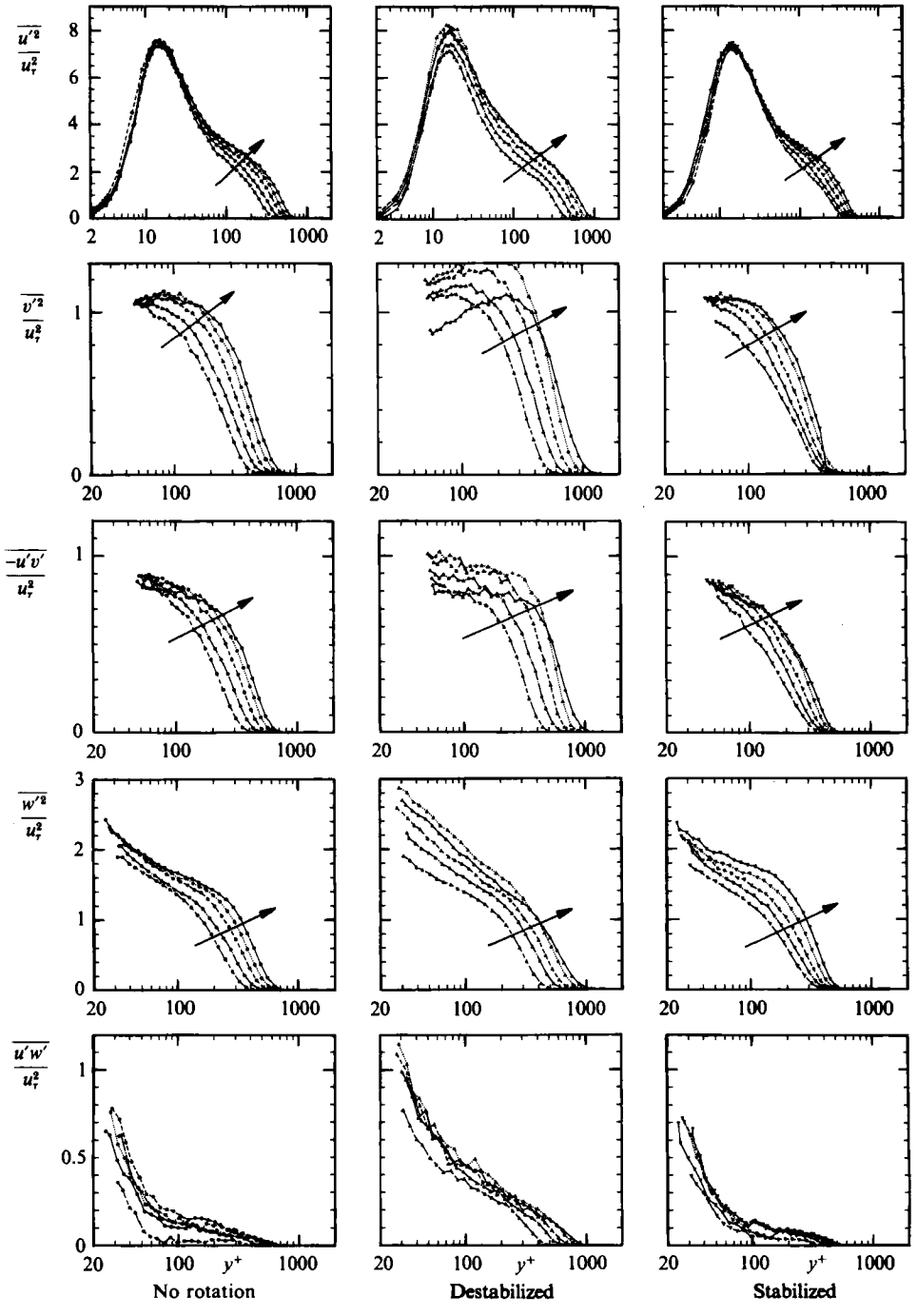

FIGURE 9. Components of Reynolds stress for $U_1 = 7.5$ m/s. Wall scaling. Arrows indicate development with streamwise distance for each rotation condition.

rotation and is also the least likely to suffer from the effects of overstimulation. Detailed sets of turbulence-quantity profiles have been made in this layer as it develops with streamwise distance. Profiles have also been measured at the last streamwise station for the other two free-stream velocities.

The development of streamwise turbulence intensity in wall coordinates is shown in figure 9 for the layers with a free-stream velocity of 7.5 m/s. As mentioned in §3 the wall distance was determined by viewing the wire and its image in the wall with a microscope. However, very close to the wall even a small bow in the wire makes if difficult to define the effective centre of the wire with precision so that the same profile measured with two different wires may not collapse exactly in this region. A measure of experimental uncertainty is how repeatable a measurement is. In order to get an estimate of the repeatability a particular zero-rotation profile was measured on 5 separate occasions. The peak turbulence intensities close to the wall were the same within $\pm 2\,\%$. Within the uncertainty in wall distance and within the repeatability of the measurements, the results for the zero-rotation and stabilized layers at each station have the same distribution from the wall out to where logarithmic behaviour of the mean-velocity profiles is observed. In particular the same peak values of $\overline{u'^2}/u_\tau^2$ between 7.3 and 7.6 are observed just outside the sublayer at $y^+ \approx 15$. The distributions for the destabilized layers show strong similarity only for the first two streamwise stations. The peak values increase to around 8.0 with streamwise development. We were disturbed by this result since the deviations occur close to the wall where the flow should be universal. Many of these profiles were repeated on a number of occasions yet much the same results were obtained.

Crossed-wire measurements corresponding to those taken with the normal wire are also shown in figure 9. The repeatability of the normal Reynolds stresses was found by experiment to be similar to that observed for the normal wire, i.e. $\pm 2\,\%$, but positive deviations of up to 8 % are observed from the normal wire estimates of $\overline{u'^2}/u_\tau^2$ in the regions close to the wall. The differences are most evident when the probe is aligned to measure spanwise velocity components. In this configuration the differences close to the wall are probably caused by mean shear across the filaments. When the probe is aligned to measure the velocity component normal to the wall much of the differences can be explained by errors in wall distance since the effective centre of the crossed-wire filaments is less well defined than that of the normal wire. The repeatability of the Reynolds stresses near the wall was found to be poorer, around $\pm 5\,\%$, for a given probe geometry. The authors found that variations as large as $\pm 10\,\%$ were experienced in the same flow when the geometry was altered.

Near the beginning of the region where the mean-velocity profiles exhibit logarithmic behaviour, the distributions of $\overline{v'^2}/u_\tau^2$ for the zero-rotation and stabilized layers appear to peel off from values around 1.1. A region of almost constant value can be seen to emerge with streamwise development. The measurements of the Reynolds shear stress $-\overline{u'v'}/u_\tau^2$ are lower than expected close to the wall. Assuming that there is a small region of constant shear stress in the layer from the wall outwards, we would expect to find the value of non-dimensionalized shear stress to be close to unity provided that viscous stresses are negligible. In the region of validity of the logarithmic law of the wall the viscous component is less than 6 %. Therefore these results at 7.5 m/s could be in error by up to 10 %. However, extrapolation of the profiles towards the wall does result in the expected value. The observation could imply a low-Reynolds-number boundary-layer phenomenon, i.e. the shear stress falls off rapidly from very close to the wall. Although there is a lack of reliable data in this form in the literature

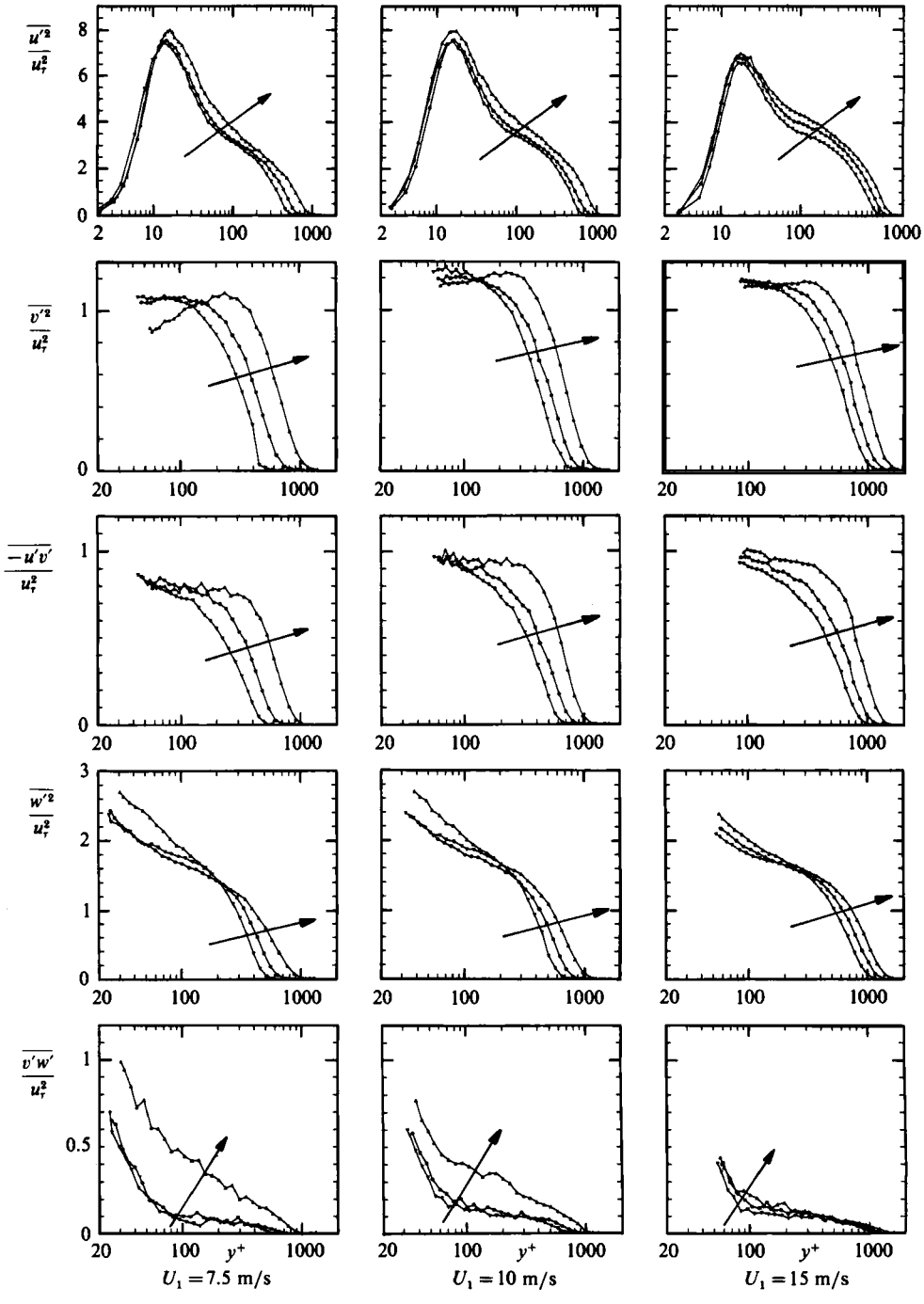

FIGURE 10. Components of Reynolds stress at last station for three free-stream velocities. Wall scaling. Arrows indicate the effect of rotation from −60 r.p.m., 0 r.p.m, to +60 r.p.m.

for low-Reynolds-number turbulent boundary layers, the result could also be a property of the probe or instrumentation under these conditions (see Willmarth & Bogar 1977 for some disturbing experiences with crossed-wire probes close to the wall). It is likely that any errors would be of similar magnitude for the rotating-layer profiles so that our data are likely to show at least the correct trends. In the stabilized and zero-rotation layers a small region of almost constant shear stress emerges near the wall with streamwise development. This is more evident in the zero-rotation layers. As is consistent with the normal-wire results, only the profiles at the first two stations for the destabilized layers show any similarity to the corresponding zero-rotation and stabilized-layer profiles of $\overline{v'^2}/u_\tau^2$ and $-\overline{u'v'}/u_\tau^2$. The values of the shear stress in this layer remain approximately constant over a much larger region which grows with streamwise development.

It is difficult to provide an estimate of the errors associated with the measurements of $\overline{w'^2}$ and $\overline{u'w'}$. Close to the wall they are most probably distorted by the effects of mean shear across the wire filaments. It seems that the values of $\overline{u'w'}$ are subject to gross errors for $y^+ < 100$. Ideally $\overline{u'w'}$ should be zero in the stabilized and zero-rotation layers. It can be shown from the Reynolds stress tensor that even slight angular misalignment of the probe from its calibration orientation can lead to quite large values of this quantity due to contributions from the relatively large u' and w' fluctuations experienced near the wall. The consistently higher values of $\overline{u'w'}$ seen in the destabilized layers can be explained by the presence of the vortices (see §4.2). The development of $\overline{w'^2}/u_\tau^2$ follows the trend observed for $\overline{u'^2}/u_\tau^2$ for all layers. Within the relatively large uncertainty of these measurements the profiles peel off from what could be universal values of this quantity near the wall where logarithmic variation of the mean-velocity profiles begins. Once again the destabilized-layer profiles show considerable scatter.

The results at the last station for each of the free-stream velocities are shown in figure 10. Here a direct comparison can be made with the quantities measured under different rotation conditions. The stabilized-layer profiles of $\overline{u'^2}/u_\tau^2$ lie slightly below the zero-rotation profiles in the turbulent wall region. Deviations from the zero-rotation profiles are observed in the destabilized layers for $y^+ < 15$. Within the uncertainty of wall distance all the profiles collapse in the region closer to the wall. The lower peak turbulence intensities in the 15 m/s layers are probably caused by the poorer spatial resolution of the hot-wire filaments. The profiles of $\overline{v'^2}/u_\tau^2$ and $-\overline{u'v'}/u_\tau^2$ remain roughly constant over a region that corresponds to where the mean-velocity profiles exhibit logarithmic behaviour. As is consistent with the mean-velocity profiles, this region is longer for the destabilized layers and slightly shorter for the stabilized layers. At the higher free-stream velocities the Reynolds stress $\overline{u'v'}$ tends closer to expected values. For $\overline{w'^2}/u_\tau^2$ the zero rotation and stabilized profiles look similar close to the wall while larger values are observed in the destabilized layers. In the outer region of the layers the distributions of $\overline{w'^2}/u_\tau^2$ resemble the profiles of $\overline{u'^2}/u_\tau^2$. Once again, close to the wall, the values of $\overline{u'w'}$ appear to be affected by the shear across the wire filaments. The larger values of $\overline{u'w'}$ in the destabilized layers are only evident at the lower free-stream velocities.

The scaling of turbulence quantities in the outer region of a turbulent boundary layer is more complex. According to the Townsend (1976) Reynolds-number-similarity hypothesis, in the outer region of the flow the broad-band turbulence quantities should scale with u_τ and an outer lengthscale, e.g. the boundary-layer thickness δ. The Townsend hypothesis is valid strictly only in the limit of high Reynolds number. Nevertheless it is interesting to consider how well our low-Reynolds-number data

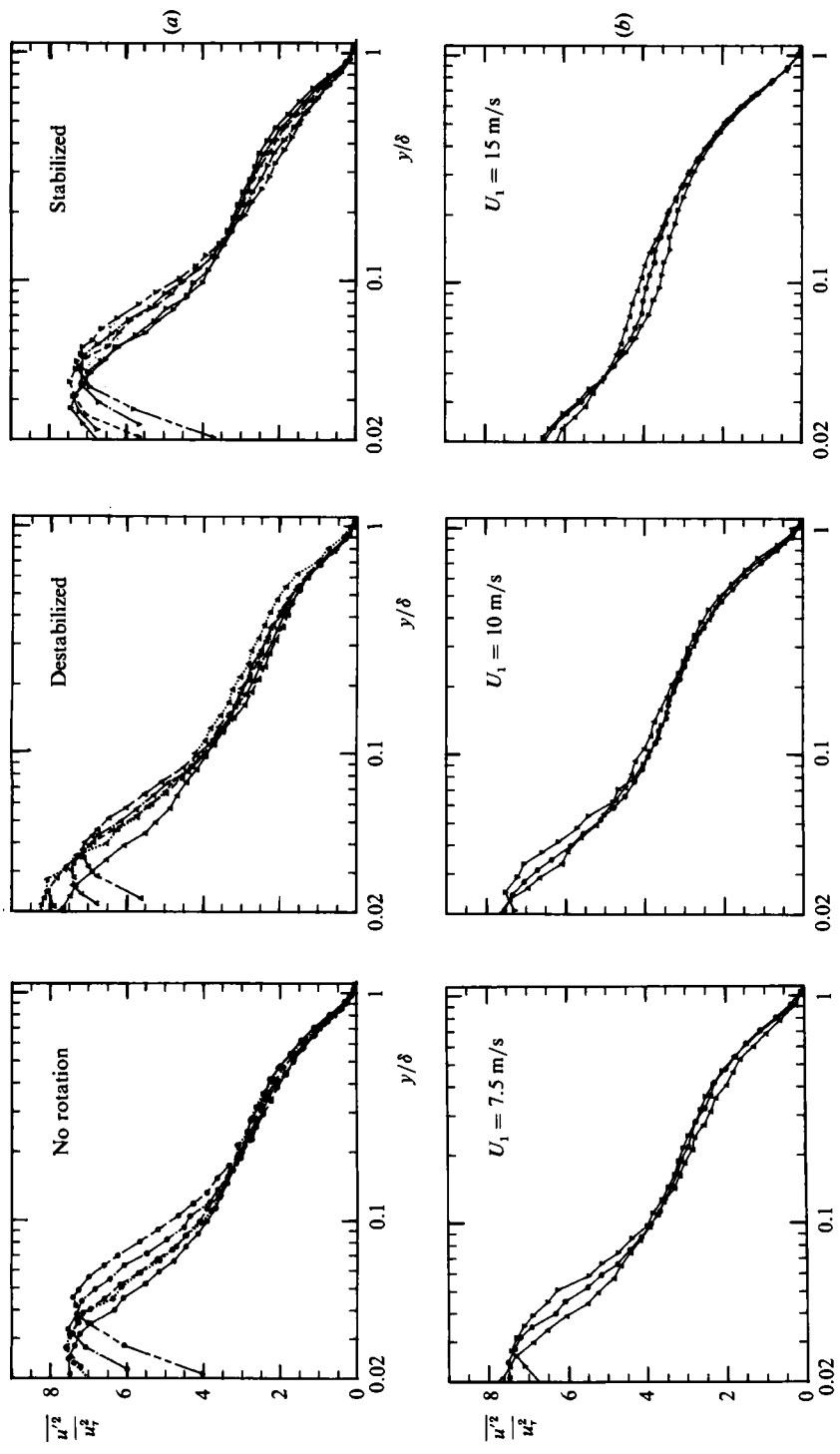

FIGURE 11. Streamwise turbulence intensities. Outer flow scaling. (*a*) Development with streamwise distance for each rotation condition, $U_1 = 7.5$ m/s. (*b*) Last station, three rotation conditions at each free-stream velocity.

might scale with outer-flow variables. The development of the streamwise turbulence intensity using outer-flow scaling is shown in figure 11(*a*). The zero-rotation-layer profiles show a reasonable degree of collapse for values of y/δ greater than about 0.2 and there is only a slight trend with increasing development. The stabilized-layer data show a slightly larger trend. However, the destabilized-layer data exhibit a higher degree of linearity and appear to collapse down to a value of y/δ of about 0.1. This could be because the destabilized layer is more developed and has a larger turbulent wall region as noted in the previous section. The results at the last station showing the effect of rotation for each free-stream velocity are shown in figure 11(*b*). The results at 7.5 and 10 m/s show a high degree of similarity while some variation is seen in the results at 15 m/s. Similar trends are observed for the other turbulence quantities with outer-flow scaling but these are not shown.

In summary, except for the scatter in the destabilized-layer results, the inner region of the layers follow wall scaling. Regions of constant $\overline{v'^2}$ and $-\overline{u'v'}$ emerge with streamwise development and correspond with where the mean-velocity profiles exhibit logarithmic behaviour. With outer-flow scaling a high degree of similarity is seen in all $\overline{u'^2}$ profiles. It appears that unlike the mean-velocity profiles, the scaling of the turbulence quantities is not significantly altered by rotation. This is a surprising result. The effects of positive and negative rotation on the turbulence quantities appear to be similar to the effects of increased and decreased streamwise development.

4.1.3. *Spectra*

The power-spectral densities of signals produced by turbulence give an indication of the distribution of turbulent energy among the scales. To investigate further the effects of rotation, streamwise energy spectra have been measured in the layers at the last streamwise station for the free-stream velocity of 7.5 m/s. Following Perry & Abell (1977), the spectra are presented in the non-dimensional form $\phi(ky)/u_\tau^2$ *vs.* ky, where

$$\int_0^\infty \phi(ky)\,\mathrm{d}(ky) = \overline{u'^2}.$$

Here $\phi(ky)$ is the non-dimensional spectrum function and k is the non-dimensional wavenumber, calculated by assuming the Taylor hypothesis of a frozen turbulence pattern, i.e. $k = 2\pi f/U_c$, where U_c is assumed to be the local mean velocity.

From dimensional reasoning and region-of-overlap arguments applied to functional forms, Perry & Abell proposed that in the turbulent wall region a universal wall structure exists in which the spectrum function for the low-wavenumber region of the streamwise turbulence intensity is given by a -1 power law. Our spectral measurements are shown in figure 12(*a*) and there is clearly no region where the spectra show a -1 power law. Perry & Abell tentatively set the limit for the existence of the universal wall structure in a pipe as $y < 0.1y/r$ and $y > 100\nu/u_\tau$. Assuming that the boundary-layer thickness is equivalent to the pipe radius r for scaling purposes, then only at the highest Reynolds numbers do our layers satisfy their criterion for the existence of a universal wall structure. At the low Reynolds numbers of our layers the concept of a universal wall structure does not appear to be applicable. However the spectra do appear to be confined within a $-\frac{5}{3}$ power-law envelope.

Figure 12(*b*) shows a direct comparison between spectra obtained under different rotation conditions for a range of common dimensionless wall distances. The spectra measured in the viscous wall region are essentially the same for the three flows and

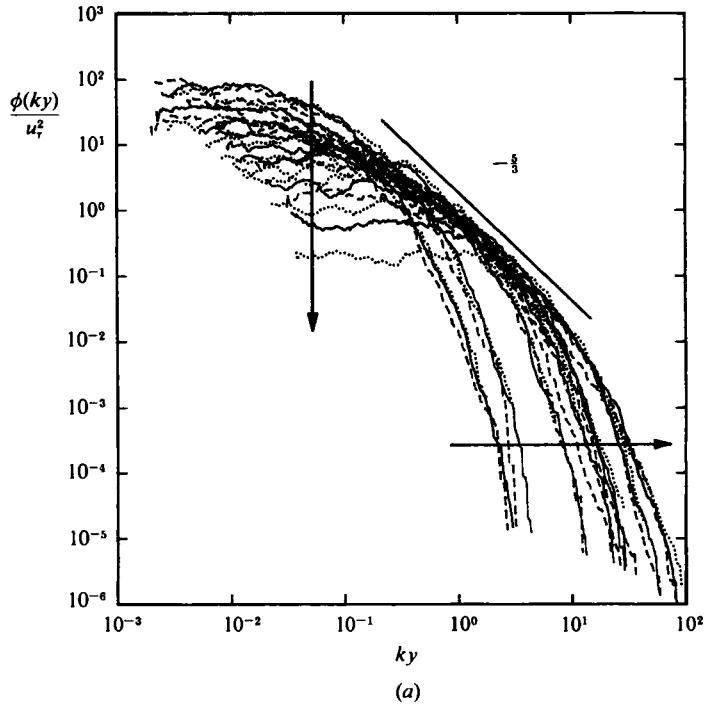

FIGURE 12(a). For caption see opposite page.

confirm the observation from the broadband results that the flow here is unaffected by rotation. Further from the wall the spectra demonstrate that it is the low-wavenumber spectral components alone that are responsible for the changes in the streamwise turbulence intensity due to rotation (see figure 10). The high-wavenumber regions are common to the three layers independent of rotation. Hunt & Joubert (1979) obtained similar results for fully developed curved-duct flow, i.e. only the low-wavenumber spectral components were affected by surface curvature. The outer (concave) wall low-wavenumber spectra have more energy and those of the inner (convex) wall have less energy than the corresponding straight-duct results. For our results the affected region of wavenumbers is given approximately by $1/k\delta$ greater than 0.5.

4.2. *Spanwise measurements*

As mentioned in §3 the spanwise variation of C_f' is around $\pm 2\frac{1}{2}\%$ for the zero-rotation layers. However, much larger variations are observed in the layers subject to spanwise rotation. The results of a series of traversing Preston-tube investigations throughout the central half-height of the duct are shown in figures 13(*a*) and (*b*). Large variations which are almost spatially periodic in the spanwise direction can be observed in the destabilized layers. As with any two-dimensional turbulent boundary layer, ideally the destabilized layers should not exhibit spanwise variations of mean-flow quantities. The increased sensitivity in the presence of the Coriolis force probably causes the flow structures to lock into weak upstream disturbances (e.g. caused by wind-tunnel screens, see Bradshaw 1965) as the layer develops. The stabilizing influence of the Coriolis force should dampen any disturbances and near the duct centreline the spanwise variations of C_f' in the stabilized layer are indeed slightly less than those of the zero-rotation layer. The influence of secondary flows is thought to cause the variation of C_f' away from the centreline in the stabilized layer and will be

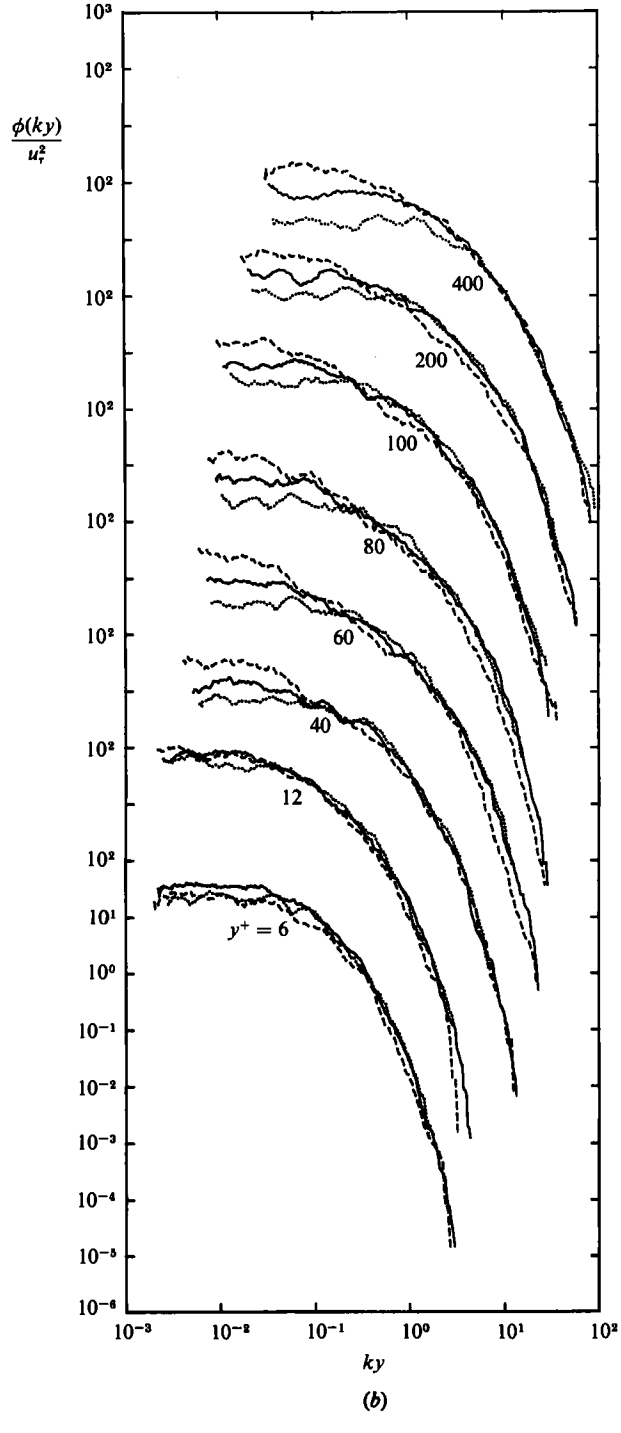

FIGURE 12. Comparison of streamwise-energy spectra under different rotation conditions, last station, $U_1 = 7.5$ m/s. (*a*) Arrows indicate effect of increasing y^+ from end of sublayer. Spectra appear confined to $-\frac{5}{3}$ power-law envelope. (*b*) Displacement of data shows it is the low-wavenumber region ($1/k\delta \gtrsim 0.5$) alone that is affected by rotation. (Common y^+ values labelled). – – –, destabilized, ——, no rotation, · · · ·, stabilized.

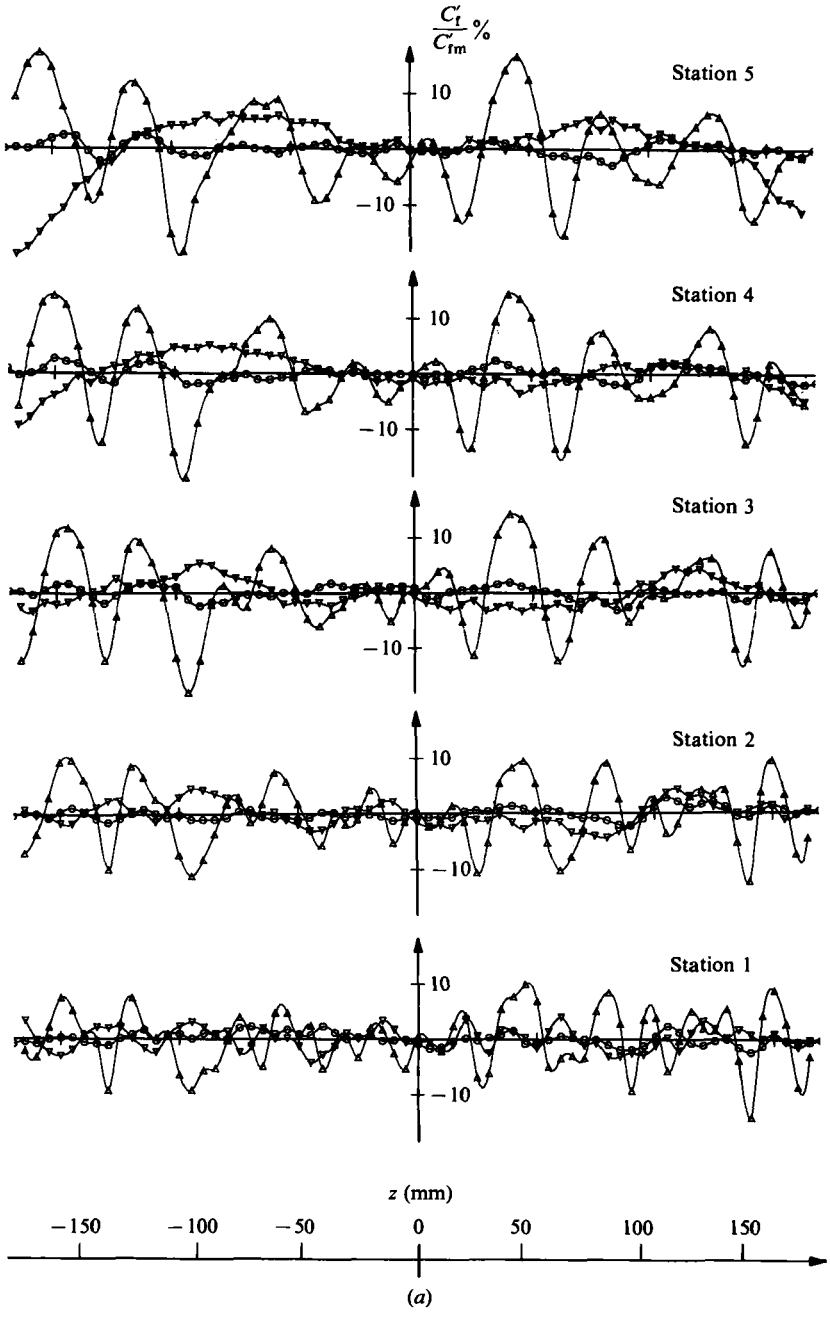

(a)

FIGURE 13(a). For caption see opposite page.

discussed in §4.3. The spanwise coordinate z in figures 13(a) and (b) has not been non-dimensionalized by the layer thickness since δ varies with C_f' across the destabilized layers. For example at $z = 45$ mm, which is a C_f' maximum, $\delta \approx 33$ mm (see figure 15), while at $z = 65$ mm, which is a C_f' minimum, $\delta \approx 42$ mm. Even if a representative thickness was defined (e.g. the average across the layer), this quantity would grow with streamwise development and depend on the free-stream velocity. Normalizing z with this quantity would therefore hide the following features: (i) the spanwise

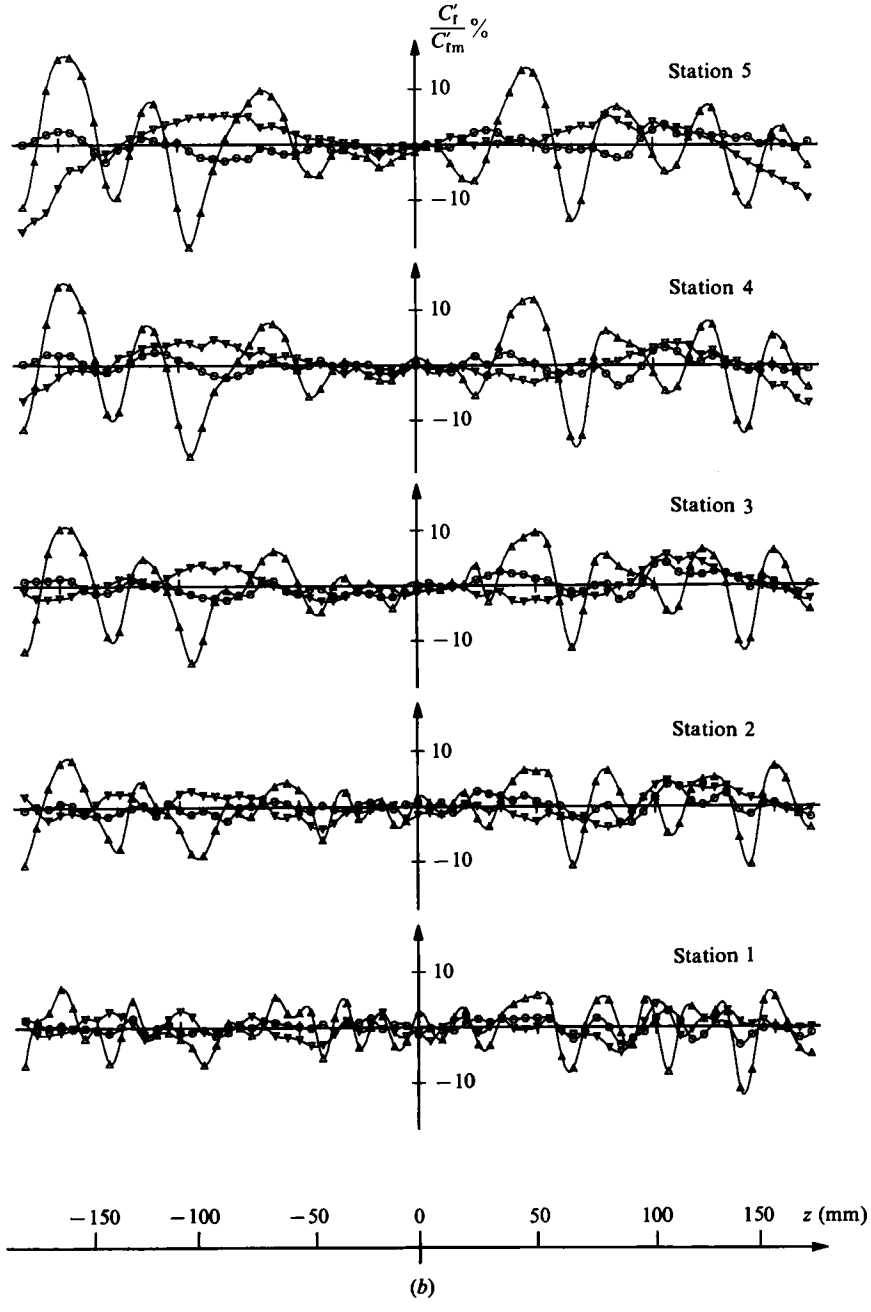

FIGURE 13. Spanwise variation of C_f' across central half-height of layer. Results normalized with mean value. Streamwise stations labelled. (*a*) $U_1 = 7.5$ m/s, (*b*) $U_1 = 10$ m/s. (Symbols as for figure 3.)

locations of the peaks are very nearly invariant with streamwise development; and (ii) there are negligible differences in the spanwise spacings for the two free-stream velocities. However, it is noted that the spanwise spacing of the peaks at the last station is approximately half the layer thickness (see figure 15). Also, the amplitudes of the spanwise variations grow with streamwise development at a decreasing rate.

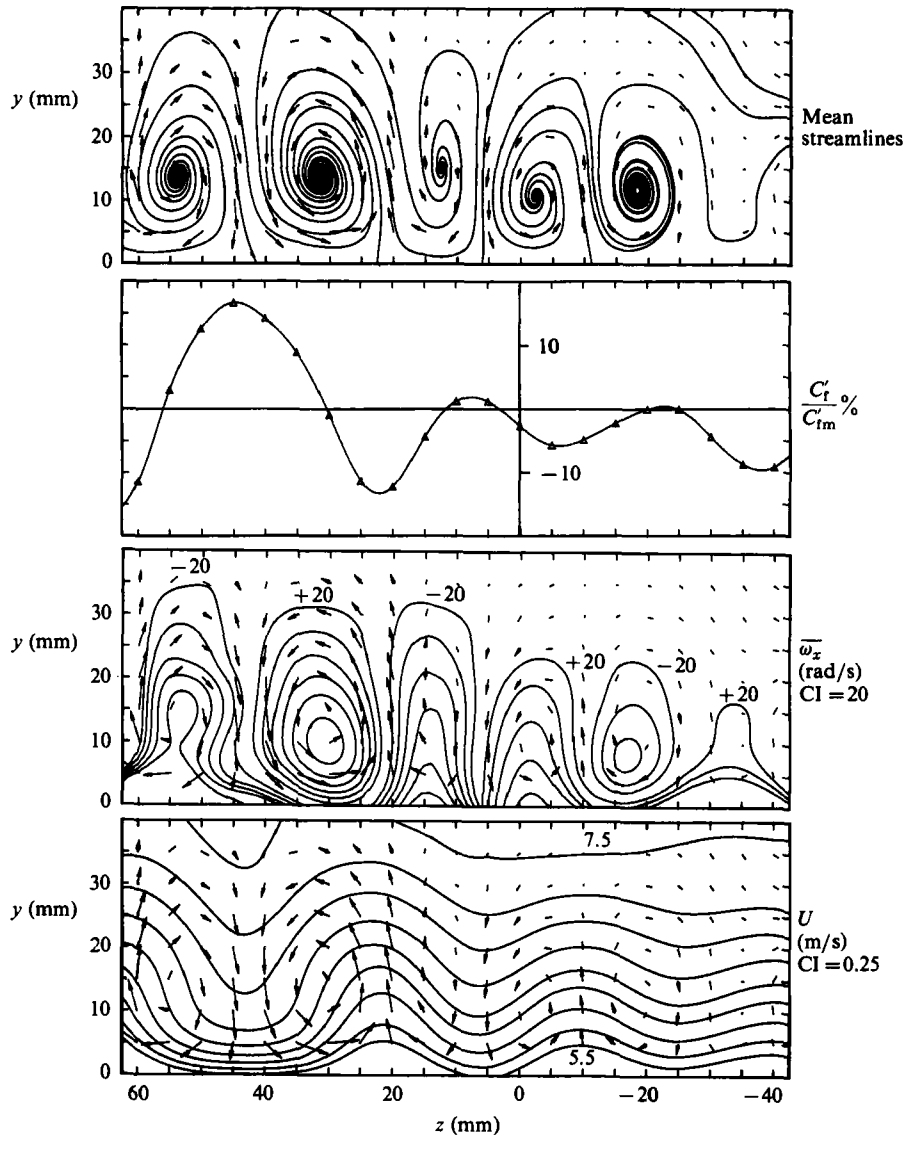

FIGURE 14. Mean-velocity-vector field in (y, z)-plane of destabilized layer. Last station, $U_1 = 7.5$ m/s, mean $u_\tau = 0.363$ m/s across central half-height of layer. Length of arrowheads corresponds to 0.0625 m/s. Streamwise flow is out of page. Integrated streamline pattern and contours of mean streamwise vorticity ($\overline{\omega_x}$), mean streamwise velocity U and Reynolds-stress components ($\overline{u'^2}$, $\overline{v'^2}$, $\overline{w'^2}$, $-\overline{u'v'}$, $\overline{u'w'}$) superimposed. Variation of C_f' also shown. CI = contour increments.

The theoretical analysis of Görtler (1940) shows that the centrifugal instability of a laminar boundary layer on a concave wall should lead to a system of streamwise vortices with a definite spanwise wavenumber. In an experimental investigation Tani (1962) found that the spanwise wavenumber was independent of the free-stream velocity. He suggested that the observed invariance of the wavenumber could be a particular feature of his apparatus. Bippes (1972) found that the spanwise spacing

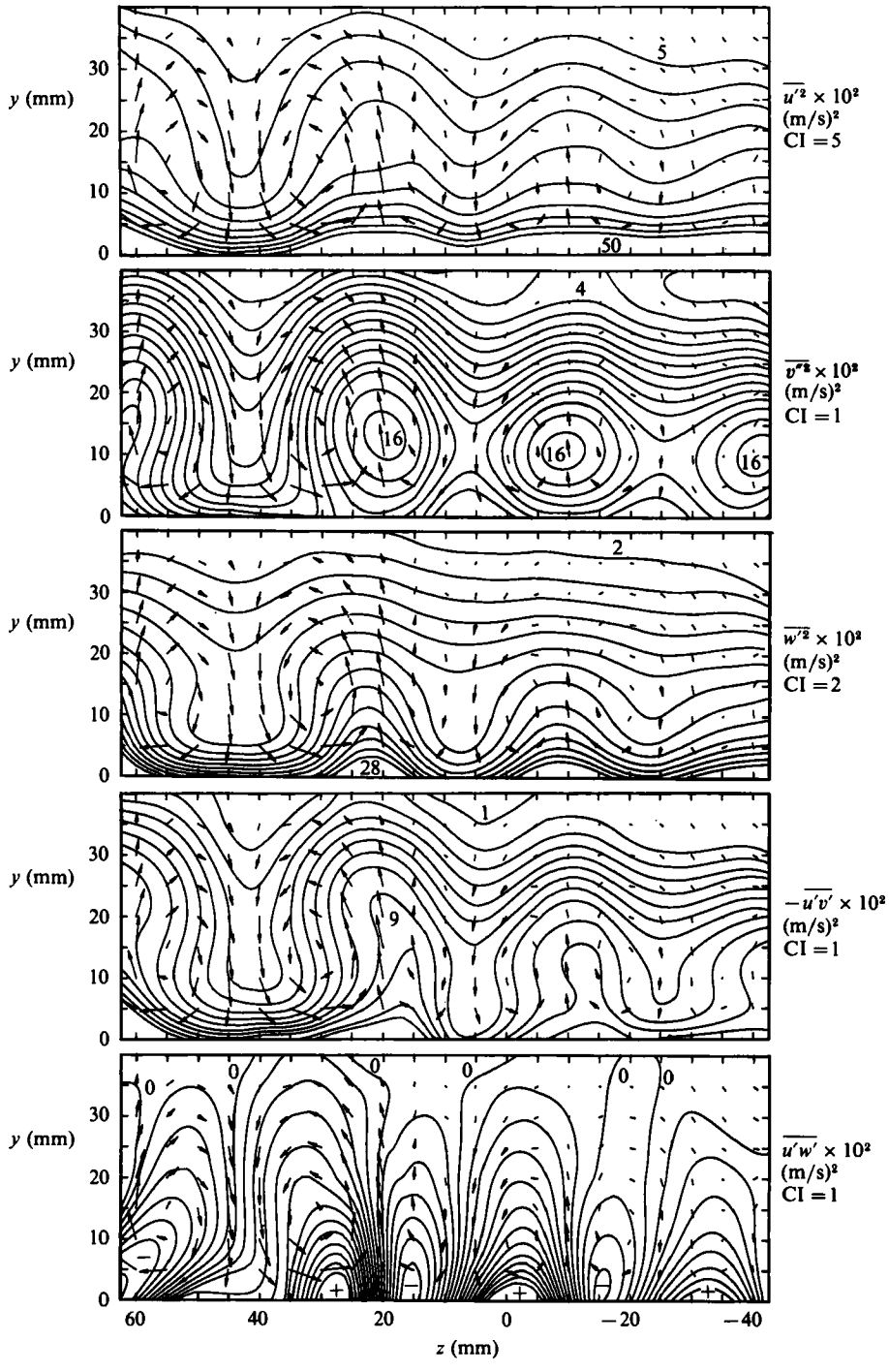

FIGURE 14 (continued). For caption see opposite page.

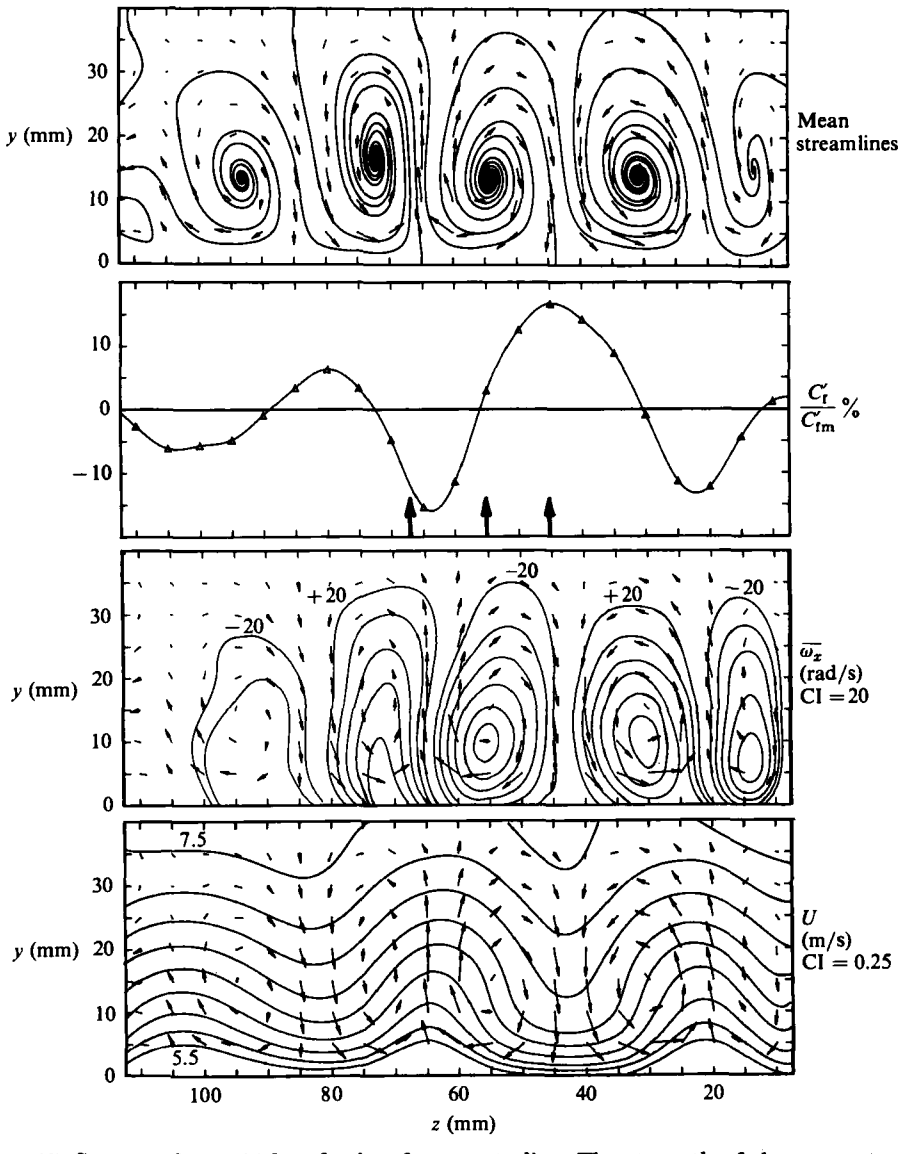

FIGURE 15. Same as figure 14 but further from centreline. The strength of the mean-streamline pattern and the contours correlate strongly with the C_f' variation. Arrows below skin-friction distribution indicate spanwise location of profiles in figure 17.

of the vortices depends on the nature of disturbances in the free stream. By making the free stream as isotropic as possible he showed that the most amplified wavelength predicted by the theory could be observed experimentally. Swearingen & Blackwelder (1983) perturbed the various parameters thought to affect the spanwise spacing of the vortices and showed that the spacing is most strongly dependent on the nature of the final wind-tunnel screen. For turbulent boundary layers on a concave wall Tani also observed spanwise variations in the mean velocity at a constant height above the wall. He suggested that the variation could be explained by the presence of longitudinal vortices in the mean flow analogous to the Taylor–Görtler vortices in the laminar boundary layer. So & Mellor (1972) observed similar variations. Smits

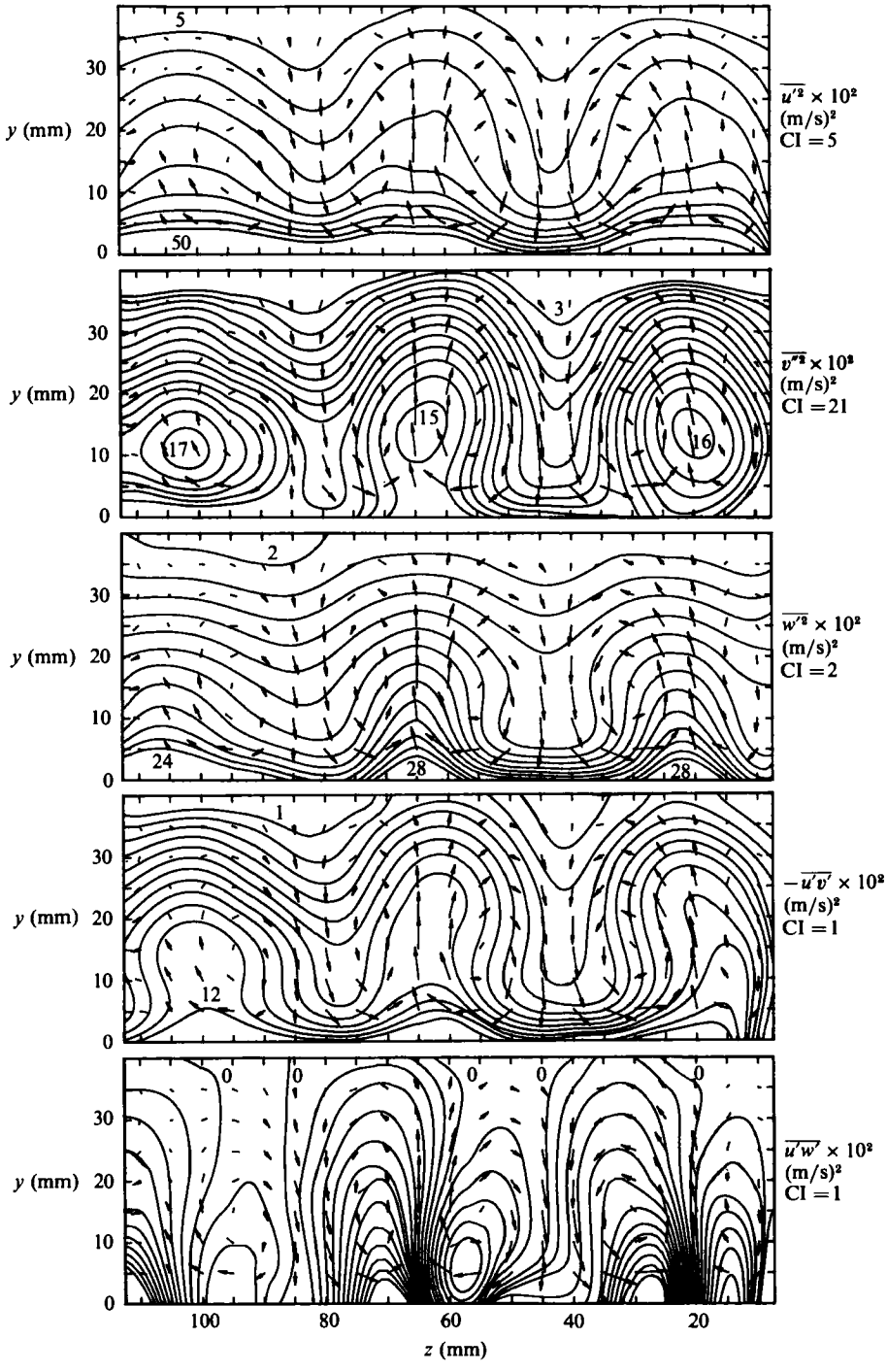

FIGURE 15 (continued). For caption see opposite page.

et al. (1979) also observed spanwise variations in C_f' and Reynolds stresses downstream of an impulsive change in wall curvature. Following Tani, these authors suggest the existence of streamwise vortices in the mean flow.

We set out to test this idea in our rotating layers by making measurements in a cross-stream plane normal to the wall. After calibration for the velocity component normal to the wall, the crossed-wire probe was traversed through the layer along rows at 5 mm intervals from the wall and mean values were obtained at 5 mm intervals along each row so that the data lay on a square grid. Measurements of the Reynolds stresses were also recorded. The measurements of the spanwise-velocity components were obtained subsequently using the same techniques. Hot-wire drift was monitored by returning the probe to its initial position after traversing each row. The mean-velocity vectors shown in figures 14 and 15 clearly show an array of vortex-like structures of alternate sign. As far as the authors are aware, this is the first time that direct evidence has been presented for the existence of longitudinal vortex-like structures in the mean flow coinciding with spanwise variations of mean-flow quantities in turbulent boundary layers. The C_f' maxima correspond to regions where the mean flow is directed towards the wall and the minima where the flow is leaving the wall. The magnitudes of the mean-flow vectors are related to the size of the C_f' variations which are also shown in figures 14 and 15. In particular the pattern is weak near the centreline of the duct where the variations in C_f' are small. The authors suggest that the relationship between the vectors and the spanwise-C_f' variations is almost certainly the same at the other streamwise stations.

It is necessary to comment on the way that the data have been processed. The length of the vector arrowheads corresponds to a cone-angle variation of about half a degree of arc away from the mean values along each row. The cone-angle variation is then only a little larger than the uncertainty in the alignment of the probe in the traverse sting. Therefore the velocity vectors were calculated from velocity perturbations about the mean values V and W along each row which were indicated from the hot-wire calibrations. The changes in the mean velocities from row to row correlate strongly with the small amount of drift experienced by the wires during the experiments. Although the data for each velocity component were collected during a single continous run, the data were divided into two batches with a relatively large region of overlap to facilitate plotting. The data were processed independently yet the differences between the vectors in the region of overlap are almost indiscernible.

It is interesting to consider what the mean-streamline pattern might look like surrounding the vortices. It is difficult to infer the exact nature of streamlines from velocity vectors so the mean-streamline pattern has been calculated using a numerical technique. Least-squares polynomial surfaces of best fit have been applied to the data over small rectangular regions of the grid as

$$\frac{\mathrm{d}z}{\mathrm{d}t} = W(y,z), \quad \frac{\mathrm{d}y}{\mathrm{d}t} = V(y,z).$$

The equations have been integrated numerically using a second-order predictor–corrector method to give each streamline $y = f(z)$. The size of the regions for fitting the polynomials is 5×5 grid points. A total of 18 such regions have been overlaid symmetrically on each grid and 4th-order polynomials are used for the fit. A desirable feature of the polynomial fits is that slight smoothing of the experimental data is obtained. For each point along the streamlines the region whose centre is closest is the one that is used for the calculations. Up to 1000 points are used for each streamline.

The most striking feature of the mean-streamline pattern is that the flow alternately spirals in towards regions of positive streamwise vorticity and away from regions of negative vorticity. These unusual spiralling patterns could be due to uncertainties in the velocity measurements; however, the same wires and calibration methods were used to measure both velocity components. While the strength of the vortex-like patterns depends on the absolute magnitudes of the hot-wire-system sensitivities, the computed streamlines depend only on the relative magnitudes. The spiralling mean-streamline pattern must be three-dimensional from continuity considerations which implies an acceleration of the u-component of velocity. Since these measurements have only been taken at the last station we do not have an independent confirmation of the implied acceleration from continuity considerations. The authors suggest that the mean flow consists of spiralling streamlines which surround continuous longitudinal vortices and that the spiralling is related to the growth of the C_f' variations observed in figure 13.

The streamline patterns have also been computed using slightly larger regions (7×5 grid points) for the fit which allow 5th-order polynomials to be used. Much the same results were obtained independently of how the regions were overlaid on the grid, i.e. the streamlines were seen to spiral in towards the regions of positive vorticity and out of regions of negative vorticity. Other features of the higher-order polynomial-fit solutions, such as limit-cycle trajectories surrounding the vortices, were also observed. In many cases the vortex-core size indicated by the limit cycle was larger for the vortices where the flow spirals out and smaller or non-existent where the flow spirals in. This is consistent with the notions of vortex stretching and contraction. However, the authors doubt whether detailed features such as the size of vortex cores can be seriously considered with the relatively coarse grid size and techniques that have been used.

The method of approximating small regions of the grid data with polynomial surfaces of best fit has been applied to all the other quantities that were measured simultaneously. The polynomial expressions allow contours of these quantities to be calculated and related to the mean-streamline pattern. The contours of mean streamwise velocity shown in figures 14 and 15 correlate strongly with the mean-streamline pattern. For example, the contours dip towards the wall where the mean circulations induce high-velocity fluid in the outer flow towards the wall. The corrugations of the contours are also related to the strength of the patterns. In particular the contours are flatter near the centreline where the mean motions are weaker. The contours of the Reynolds stresses $\overline{u'^2}$, $\overline{w'^2}$ and $-\overline{u'v'}$ are also strongly related to the pattern and look similar to those of the mean velocity. The contours extend towards the free stream as the turbulent motions close to the wall are convected outwards by the action of the vortex-like structures and the contours approach the wall where less turbulent outer-flow fluid is brought inwards. The contours of $\overline{v'^2}$ have similar properties with the exception that the maxima form closed contours away from the wall where the mean flow is directed outwards. This is expected since these velocity fluctuations are inhibited by the wall. The contours of $\overline{u'w'}$ are perhaps the most interesting since they undergo changes of sign. The turbulent shear stress tends to oppose the spanwise motions of the vortex-like structures near the wall.

It is worth noting that the peak positive values of $\overline{u'w'}$ are nearly twice as large as the magnitude of the peak negative values. The differences could be caused by a slight probe misalignment or to shear effects on the wire filaments. However, the contours of zero mean spanwise stress align very well with the region where the mean

flow is directed normal to the wall. Nevertheless the data reduction process assumes that $V = W = 0$ along each row of data and this assumption could be grossly incorrect since a small mean spanwise velocity, caused by secondary flows for example, could exist in the real flow. Streamline patterns depend on the relative velocity of the observer and our patterns could be distorted by observing the data at an incorrect velocity. Vorticity is a quantity that is invariant with the velocity of the observer. The mean streamwise vorticity has been calculated from the analytical derivatives of the polynomial expressions used to produce the mean-streamline pattern. Polynomial surfaces of best fit have been applied to the derived vorticity field in the same way as for the Reynolds stresses so that the contours shown in figures 14 and 15 could be produced. The peak amplitudes of the mean vorticity are less than 2% of the sublayer vorticity and are about 20 times the rotation rate. Both the contours of the Reynolds stresses and the contours of streamwise vorticity indicate that our mean-streamline pattern has been viewed in a reference frame that is very nearly stationary with respect to the vortices.

In a recent flow-visualization study of developing turbulent boundary layers over a concave wall, Jeans & Johnston (1982) observed large-scale structures which were about half the layer thickness in span and coherent over the height of the layer for only several layer thicknesses downstream. Spanwise mean-velocity profiles and turbulence measurements confirmed the findings of the visualization study that the appearance of the large-scale structures was sporadic and randomly positioned in space and time. Their observations suggest that these structures are strongly three-dimensional. The observations of Johnston *et al.* (1972) in fully developed rotating duct flow indicate that the time-averaged streak spacing ($\approx 100\nu/u_\tau$) is close to the value found by Kline *et al.* The large-scale roll cells, whose size is of the order of the duct width, were seen to be very unsteady and randomly positioned in space and time. Jeans & Johnston have also suggested that the spanwise variations of the mean-flow quantities observed by other workers could be caused by weak upstream disturbances introduced by screens which cause the large-scale structures to continually form at fixed spanwise positions.

From convincing flow-visualization studies Head & Bandyopadyay (1981) have shown that a turbulent boundary layer consists of a 'forest' of hairpin or Λ-vortices which become finer and more densely packed as the Reynolds number is increased. They suggest that the spanwise spacing of the vortices follows the Kline scaling. By making plausible assumptions about the distributions of these vortices Perry & Chong (1982) were able to derive a logarithmic variation for the mean flow, broadband turbulence-intensity distributions and spectra which are consistent with measured data. It is likely that the streaks observed near the wall by Kline *et al.* and the associated motions classified as bursts and sweeps are caused by these hairpin vortices. The work of Johnston *et al.* and Jeans & Johnston indicates that, although the rate of bursting may be affected, essentially the same streaky structures are seen near the wall for layers destabilized by rotation and surface curvature. It is probable that the weak rotation that we have imposed could serve merely to amplify or attenuate the ordinary structures of a turbulent boundary layer. Our spectral measurements indicate that it is only the low-wavenumber spectral components that are affected by rotation. Perhaps the mean patterns that we observe are caused by large-scale versions of Λ-vortices, for example, which form at preferred spanwise positions as they convect past our wires.

A simple kinematic model has been used to test whether the motion of such three-dimensional structures could produce an averaged pattern similar to our

results. An array of three Λ-vortices is shown in figure 16(*a*). For simplicity the vortex rods are assumed to be straight since this enables analytical integrals to be obtained for the induced velocities using the Biot–Savart law. The model is the same as that used by Perry & Chong except that a Gaussian vorticity distribution surrounding the rods has been used instead of infinitesimal filaments. Images of the rods are needed to obtain the correct boundary condition and these are not shown in the figure. All Biot–Savart integrations were calculated without regard to the extra circulation due to system rotation. It was found that an array of three structures was sufficient to approximate the asymptotic pattern near $z' = 0$ obtained by using progressively larger arrays. In order to simulate convection of the structures past our wires the component of a probability density function (p.d.f.) is assumed to be uniform in the streamwise direction. Spanwise jitter is simulated by assuming a Gaussian p.d.f. for the component in the spanwise direction. The combined p.d.f. is approximated by the discrete distribution which is shown in figures 16(*b*) and (*c*). The averaged pattern of the velocity vectors is shown in figure 16(*d*), where contours of the averaged induced-velocity perturbations in the plane normal to the vectors have been superimposed. Of course this model is very crude and does not attempt to simulate different-sized groups of interaction between the vortices. Nevertheless the averaged pattern of velocity vectors and streamwise velocity contours bear a resemblance to our mean-flow results and therefore lends credibility to the idea that the longitudinal vortices observed in the mean-flow pattern need not necessarily be the result of averaging instantaneous structures of large streamwise extent.

Computed streamlines (not shown) for the patterns in figure 16(*d*) do not have the spiralling features observed in the experimental results. The vorticity-transport equation in a rotating frame is

$$\frac{\partial \boldsymbol{\omega}}{\partial t} + \boldsymbol{U}\cdot\boldsymbol{\nabla}\boldsymbol{\omega} = (\boldsymbol{\omega} + 2\boldsymbol{\Omega})\cdot\boldsymbol{\nabla}\boldsymbol{U} + \nu\,\boldsymbol{\nabla}^2\boldsymbol{\omega}.$$

The first term on the right-hand side requires three-dimensional flow for its existence and represents the amplification or attenuation of vorticity by extension or contraction, and by tilting (i.e. rotation) of the vortex lines. The contribution from system rotation will serve to further alter any background vorticity depending on the gradient of the velocity vector along the axis of rotation. In the mean flow the extra term owing to rotation is $\Omega\,\partial U/\partial z$. Examination of figures 13 and 14 reveals that a positive streamwise velocity gradient along the rotation axis is associated with regions of positive vorticity. In these regions the mean flow is spiralling inwards, which implies that the mean vorticity is increasing with streamwise distance, owing to stretching. On the other hand a negative velocity gradient is associated with regions of negative vorticity. In these regions the mean flow spirals outwards, which implies that the mean vorticity is decreasing, owing to contraction. In terms of the Λ-vortex model one possible explanation is that fluid, i.e. vortical fluid, flows up one leg and across and down in the other leg of each instantaneous structure. There is some evidence for this. Jeans & Johnston observed horseshoe vortices in the transition phase of a laminar boundary layer over a concave surface. Examination of their figure 26 reveals that dye representing vortical fluid originally from the wall appears to accumulate on one side of the horseshoe vortices. Superposition of line sources and sinks on the vortices shown in figure 16(*a*) could produce a mean-streamline pattern that more closely resembles our experimental results.

Since the spanwise variation of C_{f}' in the destabilized layers is small near the centreline and since the values here are close to the mean value across the layer at

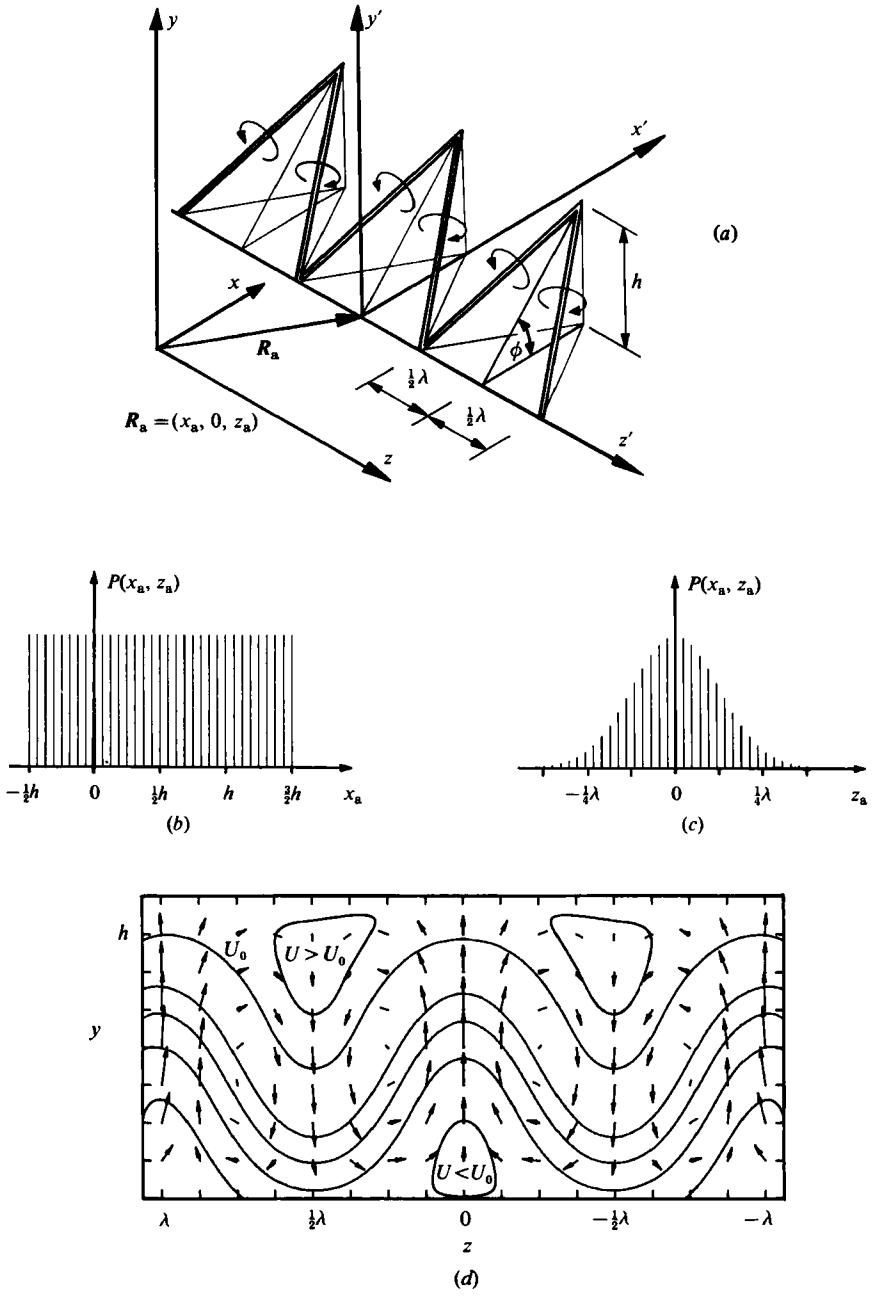

FIGURE 16. (*a*) Array of three identical Λ-vortices used to produce mean-vector field in (y, z)-plane fixed at $x = 0$. Gaussian vorticity distribution assumed uniform along each vortex rod, i.e. $\omega = \omega_0 \exp[-\frac{1}{2}(r/r_0)^2]$, where r = radial distance from rod axis, $r_0/\lambda = 1/20$, $\phi = 45°$, $h/\lambda = \frac{7}{8}$. (*b*) Uniform component of p.d.f. in streamwise direction used to simulate motion of structures past the (y, z)-plane. (*c*) Component of p.d.f. in spanwise direction used to simulate the effects of jitter. Discrete distribution approximates Gaussian p.d.f. with non-dimensional variance $\sigma_{z_a}/\lambda = \frac{1}{8}$. (*d*) Results of simulation. Mean-velocity-vector field and contours of averaged induced-streamwise velocity (arbitrary scaling) resemble experimental results shown in figures 14 and 15. (U_0 is convection velocity of vortex array.)

each streamwise station, the flow on the centreline could be representative of the layer as a whole. We propose that structures similar to those occurring away from the centreline could exist near the centreline, but subject to a larger amount of spanwise jitter. The larger jitter would further smear the flow pattern, causing the strength of the mean pattern to be diminished. Perry & Watmuff (1981) demonstrated the effect of jitter on the washout of phase-averaged patterns in the wake behind a three-dimensional ellipsoid. Given the properties of representative vortices and their PDF's of position, one could in principle derive the temporal mean-flow field.

In order to test this proposal, profiles have been measured at positions corresponding to a maximum and a minimum of C_f' and at an intermediate position through one of the vortices. The mean-velocity profiles obtained with the normal hot wire are shown in figure 17(*a*) together with the profile obtained at the centreline. Although the profiles collapse near the wall, deviations from the centreline profile occur for $y^+ > 30$ and only the profile near the minimum C_f' shows an extensive region where the mean-velocity variation is logarithmic with wall distance. The profiles at the skin-friction minimum and at the intermediate position appear to be similar for values of $y^+ < 150$ but deviate further from the wall. The profile at the skin-friction maximum has the largest deviation in the wall region and continues to the free stream with almost no identifiable wake. The authors could not find a simple statistical weighting that would produce a composite profile similar to that obtained on the centreline. Evidently a larger number of more closely spaced profiles would be needed before any definite conclusion can be drawn regarding our proposal. As a matter of interest turbulence profiles have also been measured. The features of the crossed-wire profiles (which are not shown here) can be explained in terms of cuts through the contours in figures 14 and 15. The streamwise-turbulence-intensity profiles are shown in figure 17(*b*) where the off-centreline results have been non-dimensionalized with the local value of u_τ. There is a lot of variation between them, even close to the wall. The same data are shown in figure 17(*c*) but here the centreline value of u_τ (which is close to the mean value) has been used to reduce the data. The better agreement of the results for values of $y^+ < 40$ is an unexpected result since the mean-velocity profiles appear to collapse close to the wall when non-dimensionalized with the local value of u_τ.

4.3. *Secondary flow*

As mentioned in the introduction, secondary flows generated by the top- and bottom-wall Ekman layers can have an undesirable effect on the layers developing near the centreline of a rotating duct. Speziale (1982) conducted a numerical study of fully developed laminar flow in rotating ducts of different aspect ratios. At weak-to-moderate rotation rates he showed that a counter-rotating double-vortex secondary flow forms in the transverse plane which is confined to the top and bottom walls. The diameter of the vortices is of the order of the duct width irrespective of the aspect ratio. At more rapid rotation rates the secondary flow extends further into the interior. If the rotation rate is increased further still the secondary flow in a 2:1 aspect-ratio duct splits into a pair of counter-rotating vortices while the secondary-flow vortices remain near the top and bottom walls. Speziale & Thangham (1983) have shown that for an 8:1 aspect-ratio duct the secondary flow splits into three pairs of counter-rotating roll cells which are distributed throughout the central region. A slightly stretched and asymmetric secondary flow remains near the top and bottom walls.

The numerically obtained values of the stability parameters for the onset of roll cells are in excellent agreement with the experimental and theoretical results of Hart

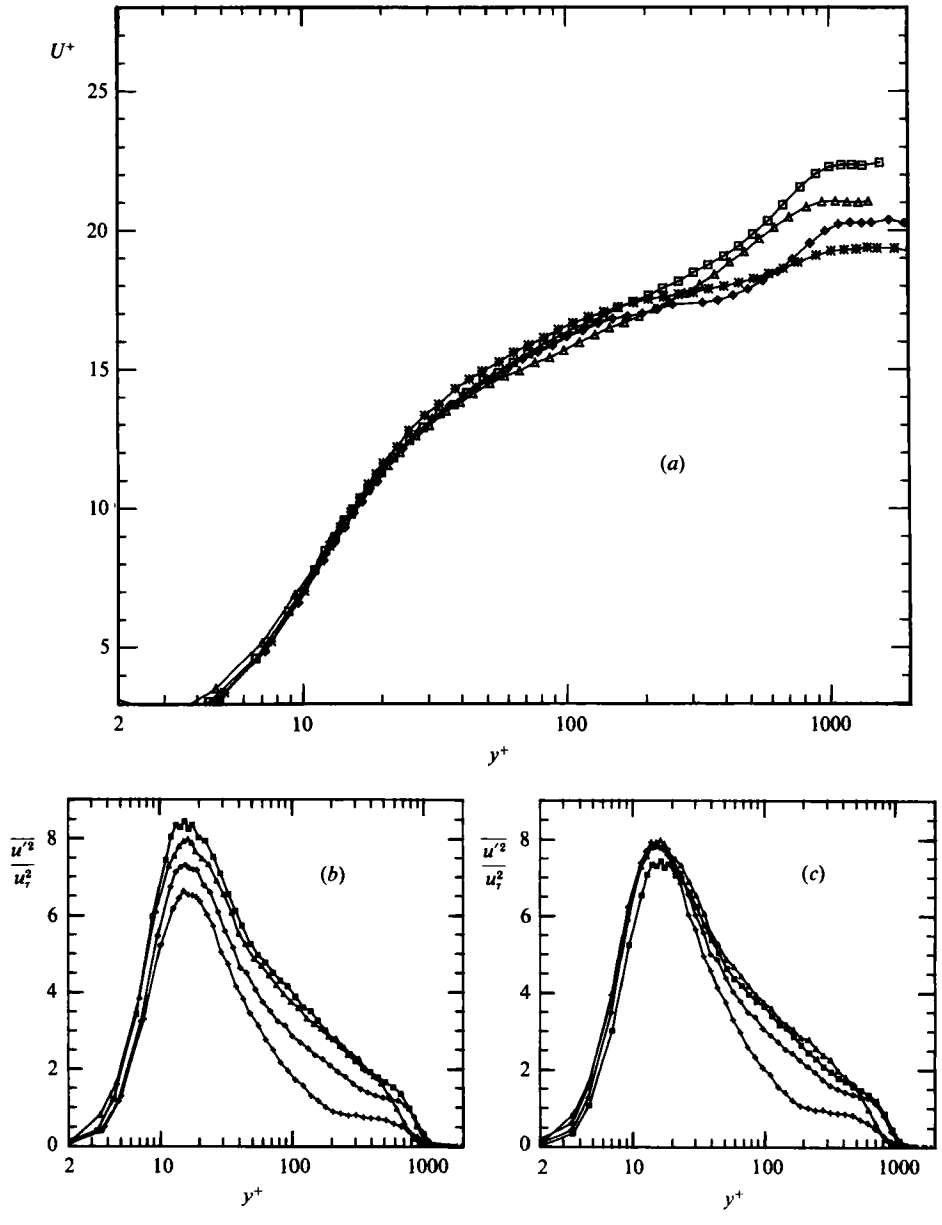

FIGURE 17. (*a*) Mean-velocity profiles obtained with normal hot wire at various spanwise positions in destabilized layer, last station, $U_1 = 7.5$ m/s. Profiles non-dimensionalized with local value of u_τ. *, near C' maximum; △, centreline profile; □, near C' minimum; ◇, between max. and min. C_t' (see figure 15 for spanwise position of profiles). (*b*) Streamwise turbulence intensity distribution corresponding to mean profiles in (*a*). Variation close to wall is evident. (*c*) Same as (*b*) but with centreline value of u_τ used to non-dimensionalize data. Agreement near the wall is better.

(1971) and Lezius & Johnston (1976). Lezius & Johnston also used a linear stability analysis with turbulence modelling to predict the onset of roll cells in fully developed turbulent duct flow which agreed very well with their experimental observations. There is strong evidence to suggest that the onset of roll cells in a large-aspect-ratio duct constitutes an instability independent of the secondary flow.

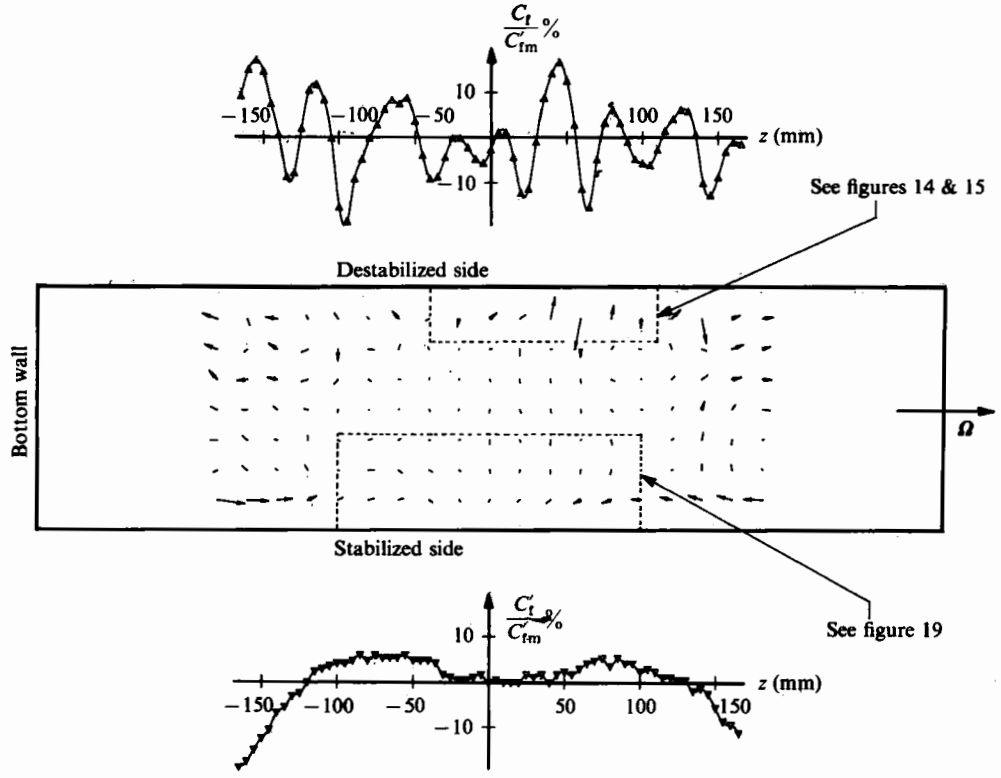

FIGURE 18. Mean velocity vectors in (y, z)-plane through duct. Last station. $U_1 = 7.5$ m/s. Length of arrowheads corresponds to 0.0625 m/s. Near extremities of measured region the pattern is consistent with weak secondary circulations near the top and bottom walls. Streamwise flow out of page.

The influence of secondary flows in our duct has been examined using the method of traversing the crossed-wire probe through the measurable region of the duct as a whole. Here it is not possible to traverse the probe completely from wall to wall, so the measurements were made on the same wall but with the two different rotation conditions applied in succession. The measurements were taken at 20 mm intervals along successive rows at 20 mm increments from the wall out to the duct centreline. The vectors for the stabilized side of the duct were reflected about the centreline to allow a composite view of the flow pattern to be produced. The results are shown for the last streamwise station at 7.5 m/s in figure 18. From the spanwise-skin-friction measurements these appear to be the conditions for which the secondary flow is strongest.

The method of surface fitting the velocities and integrating the mean-streamline patterns could not be successfully applied to the whole pattern for two reasons. Firstly the velocities in the central region of the duct are weak so that the streamlines suffer from the random effects of lack of experimental-data convergence. Secondly the vortex-like structures in the destabilized layers are more or less randomly sampled due to the relatively coarse grid size. Weak motions, almost certainly caused by secondary flows, are evident near the extremities of the measured region. However, the central region of the duct has a uniform low-turbulence free stream with negligible cross-stream velocity components. Near the stabilized side of the duct the spanwise mean-velocity components are directed towards the centreline. The motions

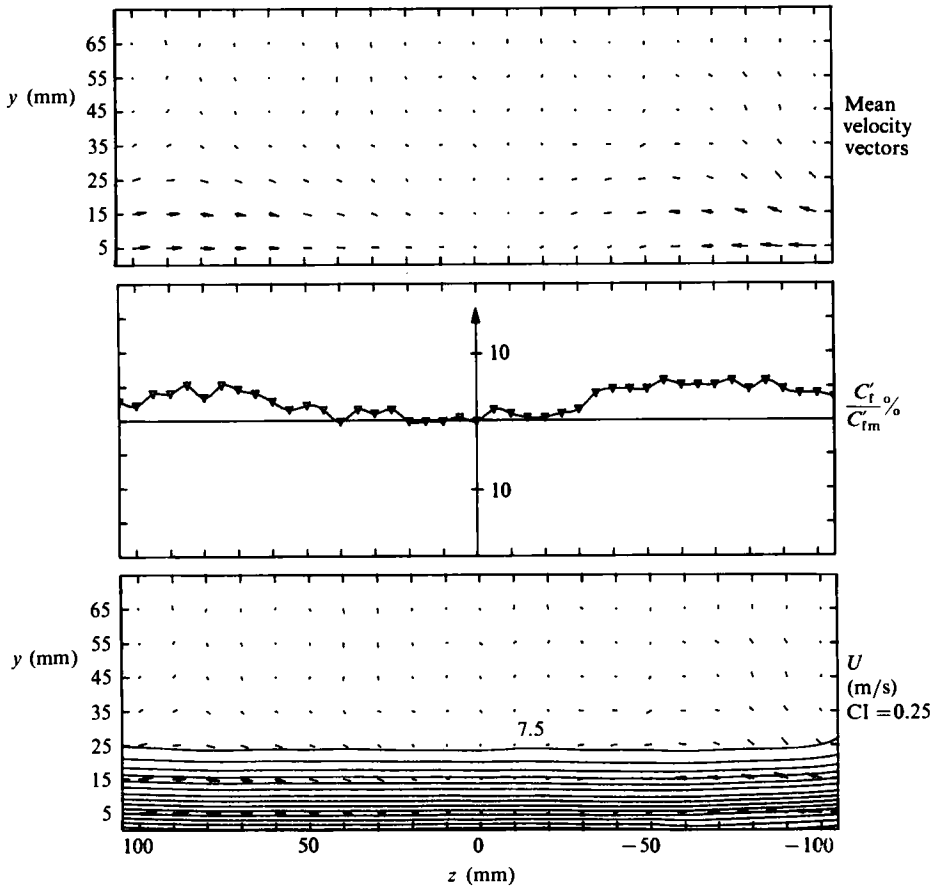

FIGURE 19. Mean-velocity-vector field in (y,z)-plane of stabilized layer. $U_1 = 7.5$ m/s, mean $u_\tau = 0.305$ m/s across half-height of layer. Length of arrowheads corresponds to 0.0625 m/s. Streamwise flow out of page. Contours of U and variation of C_f' also shown. Contours of $\overline{u'^2}$, $\overline{v'^2}$, $\overline{w'^2}$ and $-\overline{u'v'}$ (not shown) have similar degree of flatness.

appear to be related to the C_f' variations and seem to be distinct from the endwall secondary flows. For completeness, this region has also been mapped using the method of traversing the crossed-wire probe. The mean-velocity-vector field in figure 19 indicates that the spanwise velocities are confined mainly to the layer, yet the contours of the mean streamwise velocity and the Reynolds stresses $\overline{u'^2}$, $\overline{v'^2}$, $\overline{w'^2}$ and $-\overline{u'v'}$ (not shown) are parallel to the wall. The value of the shear stress $\overline{u'w'}$ at the extremities of the measured regions differ from that on the centreline by $\pm 0.07u_\tau^2$. Assuming that the cross-stream velocities are related to the spanwise variation of C_f', it appears that only the results at the last station could be affected. Since the stabilized layers exhibit an excellent momentum balance we conclude that the effect of the cross-stream motions is weak and that they have had little influence on the centreline profiles.

In the destabilized layer, the spanwise C_f' variations are clearly recognizable from the second station onwards (see figure 13). The variations in C_f' appear to fluctuate about the same value across the full measured span at each station. The spanwise locations of the peaks are nearly invariant with streamwise development. If anything a slight divergence away from the centreline is detectable at the last streamwise

station. These observations suggest that the destabilized flow has not originated from the two endwalls, but rather, like the roll cells in fully developed duct flow, the vortex-like structures are the result of the Coriolis instability and are independent of the secondary flow and therefore would exist in ducts of larger aspect ratio.

5. Conclusions

Low-Reynolds-number turbulent boundary layers developing in a zero pressure gradient have been subject to rotation about a spanwise axis. Without rotation the layers conform to documented properties and have negligible spanwise irregularities. The mean-velocity profiles effected by rotation are described in terms of a common universal sublayer and modified logarithmic and wake regions. Theories based on the analogy between buoyancy, surface curvature and rotation suggest that the deviations of the rotating-layer profiles from the logarithmic law of the wall should vary linearly with wall distance. Our data show a better fit if the deviations are assumed to vary logarithmically with wall distance. In effect this is equivalent to a modification of the constants in the logarithmic law of the wall. Compared with the zero-rotation layers, the centreline profiles of the destabilized layers exhibit logarithmic regions with lesser slopes which extend further from the wall while the relative strength of the wake components are smaller and appear to be approaching asymptotic values with less streamwise development. Opposite trends are observed in the stabilized layers.

The turbulence quantities follow an inner and outer scaling independent of rotation. The effect appears to be similar to that of increased or decreased development. Regions of constant shear stress emerge with streamwise development which correspond to where the mean flow shows logarithmic behaviour. This is most evident in the destabilized layers. Streamwise-energy spectra indicate that it is the low-wave-number spectral components alone that are affected by rotation.

Rotation has a marked effect on the wall-shear-stress distribution. For a given streamwise distance the stabilized layers have a lower value of C_f' while the destabilized layers have higher values, the effect increasing with decreasing free-stream velocity. In the stabilized layers the spanwise distribution of C_f' is uniform over the central half-height of the duct but falls towards the extremities. This effect can be attributed to large-scale secondary circulations which are confined to the extremities of the duct. The excellent momentum-balance, cross-stream mean-flow and turbulence measurements in the stabilized layers suggest that the secondary flow has had negligible influence near the centreline.

Large spatially periodic variations in C_f' are observed across the destabilized layers. However, near the duct centreline the variations are smaller and the layers have a reasonable momentum balance. Mean velocity vectors in a cross-stream plane normal to the wall clearly show an array of vortex-like structures of alternate sign which correlate strongly with the skin-friction pattern. The streamwise development of the spanwise C_f' distributions suggests that the destabilized-flow structure has not grown from the two endwalls. The numerically integrated mean-flow streamlines spiral in towards regions of positive vorticity and away from regions of negative vorticity. Contours of the Reynolds stresses dip towards the wall where less turbulent outer-flow fluid is brought inwards and extend away from the wall as turbulent wall motions are convected outwards by the action of the vortex-like structures. Using a simple three-dimensional model it is shown that the mean-flow pattern could be the result

of averaging instantaneous structures that are similar to those occurring in ordinary turbulent boundary layers, but which form at preferred spanwise positions.

Near the duct centreline the spanwise variations of C_f' are smaller, the mean-streamline pattern is weaker and the contours of the Reynolds stresses are flatter than elsewhere across the destabilized layer. Off-centreline mean-velocity profiles measured through different regions of a vortex-like structure collapse near the wall when non-dimensionalized with the local value of u_τ. Further from the wall the profiles differ from each other and from the centreline profile. Curiously the streamwise-turbulence-intensity profiles non-dimensionalized with the local value of u_τ show considerable scatter even close to the wall. However if the data are non-dimensionalized with the mean value of u_τ across the layer the profiles are in good agreement in this region. In spite of a reasonable momentum balance along the centreline the question arises as to whether the measurements here are characteristic of the layer as a whole. We have proposed that large-scale instantaneous structures, similar to those used in the model for example, could occur across the full span of the layer. The weaker mean-flow pattern near the centreline could be the result of larger spanwise jitter. However, a composite profile resembling that on the centreline could not be constructed from the limited number of off-centreline profiles. More elaborate experimental techniques would be needed to resolve the question of whether the instantaneous flow structure on the centreline is different to that elsewhere in the layer or whether the results here are simply caused by more jitter.

Even the weak vortex-like structures found on the centreline of the destabilized layers have a strong effect on the distribution of the Reynolds stresses. Similar effects could occur in less complex flows. Even in the simplest of flows, small spanwise variations of C_f' usually exist which are difficult to remove. Perhaps similar mean-flow structures are associated with these spanwise C_f' variations and are responsible for the differences, especially in turbulence quantities, measured by various workers in nominally identical flows. The need for three-dimensional measurements in complex flows has been demonstrated. What is needed are theories which take this three-dimensionality into account.

The authors wish to acknowledge the continued financial support of the Australian Research Grants Scheme, especially for the first two years during the construction and instrumentation phases of the project.

REFERENCES

Bippes, H. 1972 Experimentelle Untersuchung des laminar-turbulenten Umschlags an einer parallel angeströmten konkaven Wand. *Sitz. Heidelberger Akad. der Wiss. Math.-naturwiss. klasse 3.* (Translation *NASA TM*-75243).

Blackwelder, R. F. & Haritonidis, J. H. 1983 Scaling of the bursting frequency in turbulent boundary layers. *J. Fluid Mech.* **132**, 87.

Bradshaw, P. 1965 The effect of wind tunnel screens on nominally two-dimensional boundary layers. *J. Fluid Mech.* **22**, 679.

Bradshaw, P. 1969 The analogy between streamline curvature and buoyancy in turbulent shear flow. *J. Fluid Mech.* **36**, 177.

Bradshaw, P. 1973 Effects of streamline curvature on turbulent flow. *AGARDograph* 169.

Coles, D. E. 1962 The turbulent boundary layer in a compressible fluid. *Rand Corp. Rep.* R-403-PR, Appendix A.

Coles, D. E. & Hirst, E. A. 1969 *Proc. Computation of Turbulent Boundary Layers, 1968 AFOSR-IFP-Stanford Conference*, vol. II. Thermosciences Div. Stanford University.

GÖRTLER, H. 1940 On the three-dimensional instability of laminar boundary layers on concave walls. *NACA Tech. Memo.* 1375 – translation of *Math. Phys. Kl., Nachr. Ges. Wiss., Göttingen*, vol. 1, 1.

HART, J. E. 1971 Instability and secondary motion in a rotating channel flow. *J. Fluid Mech.* **45**, 341.

HEAD, M. R. & BANDYOPADYAY, P. 1981 New aspects of turbulent boundary-layer structure. *J. Fluid Mech.* **107**, 297.

HILL, P. G. & MOON, I. M. 1962 Effects of Coriolis on the turbulent boundary layer in rotating fluid machines. *Gas Turbine Laboratory Report No.* 69, MIT.

HUNT, I. A. & JOUBERT, P. N. 1979 Effects of small streamline curvature on turbulent duct flow. *J. Fluid Mech.* **91**, 633.

JEANS, A. H. & JOHNSTON, J. P. 1982 The effects of streamwise concave curvature on turbulent boundary layer structure. *Dept of Mechanical Engineering, Stanford University, Rep.* MD-40.

JOHNSTON, J. P., HALLEEN, R. M. & LEZIUS, D. K. 1972 Effects of spanwise rotation on the structure of two-dimensional fully developed turbulent channel flow. *J. Fluid Mech.* **56**, 533.

KLINE, S. J., REYNOLDS, W. C., SCHRAUB, F. A. & RUNSTADLER, P. W. 1967 The structure of turbulent boundary layers. *J. Fluid Mech.* **30**, 741.

KOYAMA, H., MASUDA, S., AGRIGA, I. & WATANABE, I. 1979*a* Stabilizing and destabilizing effects of Coriolis force on two-dimensional laminar and turbulent boundary layers. *Trans. ASME* A: *J. Engng Power* **101**, 23.

KOYAMA, H., MASUDA, S., ARIGA, I. & WATANABE, I. 1979*b* Turbulence structure and three-dimensionality of a rotating two-dimensional boundary layer. *2nd Intl Symp. of Turbulent Shear Flow, Imperial College, London.*

LEZIUS, D. K. & JOHNSTON, J. P. 1976 Roll-cell instabilities in rotating laminar and turbulent channel flows. *J. Fluid Mech.* **77**, 153.

MAGER, A. 1951 Generalisation of boundary layer momentum integral equations to three-dimensional flow including those of rotating systems. *NACA Tech. Note* 2310.

MOON, I. M. 1964 Effect of Coriolis force on the turbulent boundary layer in rotating fluid machines. *Gas Turbine Laboratory Rep. No.* 74, MIT.

MOORE, J. 1967 Effects of Coriolis on turbulent flow in rotating rectangular channels. *Gas Turbine Laboratory Rep. no.* 89, MIT.

PATEL, V. C. 1965 Calibration of the Preston tube and limitations on its use in pressure gradients. *J. Fluid Mech.* **23**, 185.

PERRY, A. E. 1982 *Hot-wire Anemometry*. Clarendon.

PERRY, A. E. & ABELL, C. J. 1977 Asymptotic similarity of turbulence structures in smooth- and rough-walled pipes. *J. Fluid Mech.* **79**, 785.

PERRY, A. E. & CHONG, M. S. 1982 On the mechanism of wall turbulence. *J. Fluid Mech.* **119**, 173.

PERRY, A. E. & WATMUFF, J. H. 1981 The phase-averaged large-scale structures in three-dimensional turbulent wakes. *J. Fluid Mech.* **103**, 33.

PRANDTL, L. 1931 Effect of stabilising forces on turbulence. *NACA Tech. Memo.* 625.

SMITS, A. J., YOUNG, S. T. B. & BRADSHAW, P. 1979 The effect of short regions of high surface curvature on turbulent boundary layers. *J. Fluid Mech.* **94**, 209.

SO, R. M. C. 1975 A turbulent velocity scale for curved shear flows. *J. Fluid Mech.* **70**, 37.

SO, R. M. C. & MELLOR, G. L. 1972 An experimental investigation of turbulent boundary layers along curved surfaces. *NASA CR*-1940.

SPEZIALE, C. G. 1982 Numerical study of viscous flow in rotating rectangular ducts. *J. Fluid Mech.* **122**, 251.

SPEZIALE, C. G. & THANGHAM, S. 1983 Numerical study of secondary flows and roll-cell instabilities in rotating channel flow. *J. Fluid Mech.* **130**, 377.

SWEARINGEN, J. D. & BLACKWELDER, R. F. 1983 Parameters controlling the spacing of streamwise vortices on concave walls. *AIAA 21st Aerospace Sciences Meeting, Nevada.*

TANI, I. 1962 Production of longitudinal vortices in the boundary layer along a concave wall. *J. Geophys. Res.* **67**, 3075.

TOWNSEND, A. A. 1976 *The Structure of Turbulent Shear Flow.* 2nd edn. Cambridge University Press.

WATMUFF, J. H., WITT, H. T. & JOUBERT, P. N. 1983 Effects of spanwise rotation on two-dimensional zero pressure gradient boundary layers. *IUTAM Symp. Structure of Complex Turbulent Shear Flow. IMST Marseille 1982.* Springer-Verlag.

WILLMARTH, W. W. & BOGAR, J. B. 1977 Survey and new measurements of turbulent structure near the wall. *Phys. Fluids Suppl.* **20**, S9.